# Measurement of Particle Production and Inclusive Differential Cross Sections in $p\bar{p}$ Collisions at $\sqrt{s} = 1.96$ TeV


T. Aaltonen,[24] J. Adelman,[14] T. Akimoto,[56] B. Álvarez González[t],[12] S. Amerio[z],[44] D. Amidei,[35] A. Anastassov,[39] A. Annovi,[20] J. Antos,[15] G. Apollinari,[18] A. Apresyan,[49] T. Arisawa,[58] A. Artikov,[16] W. Ashmanskas,[18] A. Attal,[4] A. Aurisano,[54] F. Azfar,[43] W. Badgett,[18] A. Barbaro-Galtieri,[29] V.E. Barnes,[49] B.A. Barnett,[26] P. Barria[bb],[47] V. Bartsch,[31] G. Bauer,[33] P.-H. Beauchemin,[34] F. Bedeschi,[47] D. Beecher,[31] S. Behari,[26] G. Bellettini[aa],[47] J. Bellinger,[60] D. Benjamin,[17] A. Beretvas,[18] J. Beringer,[29] A. Bhatti,[51] M. Binkley,[18] D. Bisello[z],[44] I. Bizjak[ff],[31] R.E. Blair,[2] C. Blocker,[7] B. Blumenfeld,[26] A. Bocci,[17] A. Bodek,[50] V. Boisvert,[50] G. Bolla,[49] D. Bortoletto,[49] J. Boudreau,[48] A. Boveia,[11] B. Brau[a],[11] A. Bridgeman,[25] L. Brigliadori[y],[6] C. Bromberg,[36] E. Brubaker,[14] J. Budagov,[16] H.S. Budd,[50] S. Budd,[25] S. Burke,[18] K. Burkett,[18] G. Busetto[z],[44] P. Bussey,[22] A. Buzatu,[34] K. L. Byrum,[2] S. Cabrera[v],[17] C. Calancha,[32] M. Campanelli,[36] M. Campbell,[35] F. Canelli[14],[18] A. Canepa,[46] B. Carls,[25] D. Carlsmith,[60] R. Carosi,[47] S. Carrillo[n],[19] S. Carron,[34] B. Casal,[12] M. Casarsa,[18] A. Castro[y],[6] P. Catastini[bb],[47] D. Cauz[ee],[55] V. Cavaliere[bb],[47] M. Cavalli-Sforza,[4] A. Cerri,[29] L. Cerrito[p],[31] S.H. Chang,[28] Y.C. Chen,[1] M. Chertok,[8] G. Chiarelli,[47] G. Chlachidze,[18] F. Chlebana,[18] K. Cho,[28] D. Chokheli,[16] J.P. Chou,[23] G. Choudalakis,[33] S.H. Chuang,[53] K. Chung[o],[18] W.H. Chung,[60] Y.S. Chung,[50] T. Chwalek,[27] C.I. Ciobanu,[45] M.A. Ciocci[bb],[47] A. Clark,[21] D. Clark,[7] G. Compostella,[44] M.E. Convery,[18] J. Conway,[8] M. Cordelli,[20] G. Cortiana[z],[44] C.A. Cox,[8] D.J. Cox,[8] F. Crescioli[aa],[47] C. Cuenca Almenar[v],[8] J. Cuevas[t],[12] R. Culbertson,[18] J.C. Cully,[35] D. Dagenhart,[18] M. Datta,[18] T. Davies,[22] P. de Barbaro,[50] S. De Cecco,[52] A. Deisher,[29] G. De Lorenzo,[4] M. Dell'Orso[aa],[47] C. Deluca,[4] L. Demortier,[51] J. Deng,[17] M. Deninno,[6] P.F. Derwent,[18] A. Di Canto[aa],[47] G.P. di Giovanni,[45] C. Dionisi[dd],[52] B. Di Ruzza[ee],[55] J.R. Dittmann,[5] M. D'Onofrio,[4] S. Donati[aa],[47] P. Dong,[9] J. Donini,[44] T. Dorigo,[44] S. Dube,[53] J. Efron,[40] A. Elagin,[54] R. Erbacher,[8] D. Errede,[25] S. Errede,[25] R. Eusebi,[18] H.C. Fang,[29] S. Farrington,[43] W.T. Fedorko,[14] R.G. Feild,[61] M. Feindt,[27] J.P. Fernandez,[32] C. Ferrazza[cc],[47] R. Field,[19] G. Flanagan,[49] R. Forrest,[8] M.J. Frank,[5] M. Franklin,[23] J.C. Freeman,[18] I. Furic,[19] M. Gallinaro,[52] J. Galyardt,[13] F. Garberson,[11] J.E. Garcia,[21] A.F. Garfinkel,[49] P. Garosi[bb],[47] K. Genser,[18] H. Gerberich,[25] D. Gerdes,[35] A. Gessler,[27] S. Giagu[dd],[52] V. Giakoumopoulou,[3] P. Giannetti,[47] K. Gibson,[48] J.L. Gimmell,[50] C.M. Ginsburg,[18] N. Giokaris,[3] M. Giordani[ee],[55] P. Giromini,[20] M. Giunta,[47] G. Giurgiu,[26] V. Glagolev,[16] D. Glenzinski,[18] M. Gold,[38] N. Goldschmidt,[19] A. Golossanov,[18] G. Gomez,[12] G. Gomez-Ceballos,[33] M. Goncharov,[33] O. González,[32] I. Gorelov,[38] A.T. Goshaw,[17] K. Goulianos,[51] A. Gresele[z],[44] S. Grinstein,[23] C. Grosso-Pilcher,[14] R.C. Group,[18] U. Grundler,[25] J. Guimaraes da Costa,[23] Z. Gunay-Unalan,[36] C. Haber,[29] K. Hahn,[33] S.R. Hahn,[18] E. Halkiadakis,[53] B.-Y. Han,[50] J.Y. Han,[50] F. Happacher,[20] K. Hara,[56] D. Hare,[53] M. Hare,[57] S. Harper,[43] R.F. Harr,[59] R.M. Harris,[18] M. Hartz,[48] K. Hatakeyama,[51] C. Hays,[43] M. Heck,[27] A. Heijboer,[46] J. Heinrich,[46] C. Henderson,[33] M. Herndon,[60] J. Heuser,[27] S. Hewamanage,[5] D. Hidas,[17] C.S. Hill[c],[11] D. Hirschbuehl,[27] A. Hocker,[18] S. Hou,[1] M. Houlden,[30] S.-C. Hsu,[29] B.T. Huffman,[43] R.E. Hughes,[40] U. Husemann,[61] M. Hussein,[36] J. Huston,[36] J. Incandela,[11] G. Introzzi,[47] M. Iori[dd],[52] A. Ivanov,[8] E. James,[18] D. Jang,[13] B. Jayatilaka,[17] E.J. Jeon,[28] M.K. Jha,[6] S. Jindariani,[18] W. Johnson,[8] M. Jones,[49] K.K. Joo,[28] S.Y. Jun,[13] J.E. Jung,[28] T.R. Junk,[18] T. Kamon,[54] D. Kar,[19] P.E. Karchin,[59] Y. Kato[m],[42] R. Kephart,[18] W. Ketchum,[14] J. Keung,[46] V. Khotilovich,[54] B. Kilminster,[18] D.H. Kim,[28] H.S. Kim,[28] H.W. Kim,[28] J.E. Kim,[28] M.J. Kim,[20] S.B. Kim,[28] S.H. Kim,[56] Y.K. Kim,[14] N. Kimura,[56] L. Kirsch,[7] S. Klimenko,[19] B. Knuteson,[33] B.R. Ko,[17] K. Kondo,[58] D.J. Kong,[28] J. Konigsberg,[19] A. Korytov,[19] A.V. Kotwal,[17] M. Kreps,[27] J. Kroll,[46] D. Krop,[14] N. Krumnack,[5] M. Kruse,[17] V. Krutelyov,[11] T. Kubo,[56] T. Kuhr,[27] N.P. Kulkarni,[59] M. Kurata,[56] S. Kwang,[14] A.T. Laasanen,[49] S. Lami,[47] S. Lammel,[18] M. Lancaster,[31] R.L. Lander,[8] K. Lannon[s],[40] A. Lath,[53] G. Latino[bb],[47] I. Lazzizzera[z],[44] T. LeCompte,[2] E. Lee,[54] H.S. Lee,[14] S.W. Lee[u],[54] S. Leone,[47] J.D. Lewis,[18] C.-S. Lin,[29] J. Linacre,[43] M. Lindgren,[18] E. Lipeles,[46] A. Lister,[8] D.O. Litvintsev,[18] C. Liu,[48] T. Liu,[18] N.S. Lockyer,[46] A. Loginov,[61] M. Loreti[z],[44] L. Lovas,[15] D. Lucchesi[z],[44] C. Luci[dd],[52] J. Lueck,[27] P. Lujan,[29] P. Lukens,[18] G. Lungu,[51] L. Lyons,[43] J. Lys,[29] R. Lysak,[15] D. MacQueen,[34] R. Madrak,[18] K. Maeshima,[18] K. Makhoul,[33] T. Maki,[24] P. Maksimovic,[26] S. Malde,[43] S. Malik,[31] G. Manca[e],[30] A. Manousakis-Katsikakis,[3] F. Margaroli,[49] C. Marino,[27] C.P. Marino,[25] A. Martin,[61] V. Martin[k],[22] M. Martínez,[4] R. Martínez-Ballarín,[32] T. Maruyama,[56] P. Mastrandrea,[52] T. Masubuchi,[56] M. Mathis,[26] M.E. Mattson,[59] P. Mazzanti,[6] K.S. McFarland,[50] P. McIntyre,[54] R. McNulty[j],[30] A. Mehta,[30] P. Mehtala,[24] A. Menzione,[47] P. Merkel,[49] C. Mesropian,[51] T. Miao,[18] N. Miladinovic,[7] R. Miller,[36] C. Mills,[23] M. Milnik,[27] A. Mitra,[1] G. Mitselmakher,[19] H. Miyake,[56] N. Moggi,[6] C.S. Moon,[28] R. Moore,[18] M.J. Morello,[47] J. Morlock,[27] P. Movilla Fernandez,[18] J. Mülmenstädt,[29] A. Mukherjee,[18] Th. Muller,[27] R. Mumford,[26] P. Murat,[18] M. Mussini[y],[6] J. Nachtman[o],[18] Y. Nagai,[56] A. Nagano,[56] J. Naganoma,[56]

K. Nakamura,[56] I. Nakano,[41] A. Napier,[57] V. Necula,[17] J. Nett,[60] C. Neu[w],[46] M.S. Neubauer,[25] S. Neubauer,[27] J. Nielsen[g],[29] L. Nodulman,[2] M. Norman,[10] O. Norniella,[25] E. Nurse,[31] L. Oakes,[43] S.H. Oh,[17] Y.D. Oh,[28] I. Oksuzian,[19] T. Okusawa,[42] R. Orava,[24] K. Osterberg,[24] S. Pagan Griso[z],[44] E. Palencia,[18] V. Papadimitriou,[18] A. Papaikonomou,[27] A.A. Paramonov,[14] B. Parks,[40] S. Pashapour,[34] J. Patrick,[18] G. Pauletta[ee],[55] M. Paulini,[13] C. Paus,[33] T. Peiffer,[27] D.E. Pellett,[8] A. Penzo,[55] T.J. Phillips,[17] G. Piacentino,[47] E. Pianori,[46] L. Pinera,[19] K. Pitts,[25] C. Plager,[9] L. Pondrom,[60] O. Poukhov*,[16] N. Pounder,[43] F. Prakoshyn,[16] A. Pronko,[18] J. Proudfoot,[2] F. Ptohos[i],[18] E. Pueschel,[13] G. Punzi[aa],[47] J. Pursley,[60] J. Rademacker[c],[43] A. Rahaman,[48] V. Ramakrishnan,[60] N. Ranjan,[49] I. Redondo,[32] P. Renton,[43] M. Renz,[27] M. Rescigno,[52] S. Richter,[27] F. Rimondi[y],[6] L. Ristori,[47] A. Robson,[22] T. Rodrigo,[12] T. Rodriguez,[46] E. Rogers,[25] S. Rolli,[57] R. Roser,[18] M. Rossi,[55] R. Rossin,[11] P. Roy,[34] A. Ruiz,[12] J. Russ,[13] V. Rusu,[18] B. Rutherford,[18] H. Saarikko,[24] A. Safonov,[54] W.K. Sakumoto,[50] O. Saltó,[4] L. Santi[ee],[55] S. Sarkar[dd],[52] L. Sartori,[47] K. Sato,[18] A. Savoy-Navarro,[45] P. Schlabach,[18] A. Schmidt,[27] E.E. Schmidt,[18] M.A. Schmidt,[14] M.P. Schmidt*,[61] M. Schmitt,[39] T. Schwarz,[8] L. Scodellaro,[12] A. Scribano[bb],[47] F. Scuri,[47] A. Sedov,[49] S. Seidel,[38] Y. Seiya,[42] A. Semenov,[16] L. Sexton-Kennedy,[18] F. Sforza[aa],[47] A. Sfyrla,[25] S.Z. Shalhout,[59] T. Shears,[30] P.F. Shepard,[48] M. Shimojima[r],[56] S. Shiraishi,[14] M. Shochet,[14] Y. Shon,[60] I. Shreyber,[37] P. Sinervo,[34] A. Sisakyan,[16] A.J. Slaughter,[18] J. Slaunwhite,[40] K. Sliwa,[57] J.R. Smith,[8] F.D. Snider,[18] R. Snihur,[34] A. Soha,[8] S. Somalwar,[53] V. Sorin,[36] T. Spreitzer,[34] P. Squillacioti[bb],[47] M. Stanitzki,[61] R. St. Denis,[22] B. Stelzer,[34] O. Stelzer-Chilton,[34] D. Stentz,[39] J. Strologas,[38] G.L. Strycker,[35] J.S. Suh,[28] A. Sukhanov,[19] I. Suslov,[16] T. Suzuki,[56] A. Taffard[f],[25] R. Takashima,[41] Y. Takeuchi,[56] R. Tanaka,[41] M. Tecchio,[35] P.K. Teng,[1] K. Terashi,[51] J. Thom[h],[18] A.S. Thompson,[22] G.A. Thompson,[25] E. Thomson,[46] P. Tipton,[61] P. Ttito-Guzmán,[32] S. Tkaczyk,[18] D. Toback,[54] S. Tokar,[15] K. Tollefson,[36] T. Tomura,[56] D. Tonelli,[18] S. Torre,[20] D. Torretta,[18] P. Totaro[ee],[55] S. Tourneur,[45] M. Trovato[cc],[47] S.-Y. Tsai,[1] Y. Tu,[46] N. Turini[bb],[47] F. Ukegawa,[56] S. Vallecorsa,[21] N. van Remortel[b],[24] A. Varganov,[35] E. Vataga[cc],[47] F. Vázquez[n],[19] G. Velev,[18] C. Vellidis,[3] M. Vidal,[32] R. Vidal,[18] I. Vila,[12] R. Vilar,[12] T. Vine,[31] M. Vogel,[38] I. Volobouev[u],[29] G. Volpi[aa],[47] P. Wagner,[46] R.G. Wagner,[2] R.L. Wagner,[18] W. Wagner[x],[27] J. Wagner-Kuhr,[27] T. Wakisaka,[42] R. Wallny,[9] S.M. Wang,[1] A. Warburton,[34] D. Waters,[31] M. Weinberger,[54] J. Weinelt,[27] W.C. Wester III,[18] B. Whitehouse,[57] D. Whiteson[f],[46] A.B. Wicklund,[2] E. Wicklund,[18] S. Wilbur,[14] G. Williams,[34] H.H. Williams,[46] P. Wilson,[18] B.L. Winer,[40] P. Wittich[h],[18] S. Wolbers,[18] C. Wolfe,[14] T. Wright,[35] X. Wu,[21] F. Würthwein,[10] S. Xie,[33] A. Yagil,[10] K. Yamamoto,[42] J. Yamaoka,[17] U.K. Yang[q],[14] Y.C. Yang,[28] W.M. Yao,[29] G.P. Yeh,[18] K. Yi[o],[18] J. Yoh,[18] K. Yorita,[58] T. Yoshida[l],[42] G.B. Yu,[50] I. Yu,[28] S.S. Yu,[18] J.C. Yun,[18] L. Zanello[dd],[52] A. Zanetti,[55] X. Zhang,[25] Y. Zheng[d],[9] and S. Zucchelli[y],[6]

(CDF Collaboration†)

[1] *Institute of Physics, Academia Sinica, Taipei, Taiwan 11529, Republic of China*
[2] *Argonne National Laboratory, Argonne, Illinois 60439*
[3] *University of Athens, 157 71 Athens, Greece*
[4] *Institut de Fisica d'Altes Energies, Universitat Autonoma de Barcelona, E-08193, Bellaterra (Barcelona), Spain*
[5] *Baylor University, Waco, Texas 76798*
[6] *Istituto Nazionale di Fisica Nucleare Bologna, [y] University of Bologna, I-40127 Bologna, Italy*
[7] *Brandeis University, Waltham, Massachusetts 02254*
[8] *University of California, Davis, Davis, California 95616*
[9] *University of California, Los Angeles, Los Angeles, California 90024*
[10] *University of California, San Diego, La Jolla, California 92093*
[11] *University of California, Santa Barbara, Santa Barbara, California 93106*
[12] *Instituto de Fisica de Cantabria, CSIC-University of Cantabria, 39005 Santander, Spain*
[13] *Carnegie Mellon University, Pittsburgh, PA 15213*
[14] *Enrico Fermi Institute, University of Chicago, Chicago, Illinois 60637*
[15] *Comenius University, 842 48 Bratislava, Slovakia; Institute of Experimental Physics, 040 01 Kosice, Slovakia*
[16] *Joint Institute for Nuclear Research, RU-141980 Dubna, Russia*
[17] *Duke University, Durham, North Carolina 27708*
[18] *Fermi National Accelerator Laboratory, Batavia, Illinois 60510*
[19] *University of Florida, Gainesville, Florida 32611*
[20] *Laboratori Nazionali di Frascati, Istituto Nazionale di Fisica Nucleare, I-00044 Frascati, Italy*
[21] *University of Geneva, CH-1211 Geneva 4, Switzerland*
[22] *Glasgow University, Glasgow G12 8QQ, United Kingdom*
[23] *Harvard University, Cambridge, Massachusetts 02138*
[24] *Division of High Energy Physics, Department of Physics, University of Helsinki and Helsinki Institute of Physics, FIN-00014, Helsinki, Finland*
[25] *University of Illinois, Urbana, Illinois 61801*
[26] *The Johns Hopkins University, Baltimore, Maryland 21218*
[27] *Institut für Experimentelle Kernphysik, Universität Karlsruhe, 76128 Karlsruhe, Germany*

[28] Center for High Energy Physics: Kyungpook National University, Daegu 702-701, Korea; Seoul National University, Seoul 151-742, Korea; Sungkyunkwan University, Suwon 440-746, Korea; Korea Institute of Science and Technology Information, Daejeon, 305-806, Korea; Chonnam National University, Gwangju, 500-757, Korea
[29] Ernest Orlando Lawrence Berkeley National Laboratory, Berkeley, California 94720
[30] University of Liverpool, Liverpool L69 7ZE, United Kingdom
[31] University College London, London WC1E 6BT, United Kingdom
[32] Centro de Investigaciones Energeticas Medioambientales y Tecnologicas, E-28040 Madrid, Spain
[33] Massachusetts Institute of Technology, Cambridge, Massachusetts 02139
[34] Institute of Particle Physics: McGill University, Montréal, Québec, Canada H3A 2T8; Simon Fraser University, Burnaby, British Columbia, Canada V5A 1S6; University of Toronto, Toronto, Ontario, Canada M5S 1A7; and TRIUMF, Vancouver, British Columbia, Canada V6T 2A3
[35] University of Michigan, Ann Arbor, Michigan 48109
[36] Michigan State University, East Lansing, Michigan 48824
[37] Institution for Theoretical and Experimental Physics, ITEP, Moscow 117259, Russia
[38] University of New Mexico, Albuquerque, New Mexico 87131
[39] Northwestern University, Evanston, Illinois 60208
[40] The Ohio State University, Columbus, Ohio 43210
[41] Okayama University, Okayama 700-8530, Japan
[42] Osaka City University, Osaka 588, Japan
[43] University of Oxford, Oxford OX1 3RH, United Kingdom
[44] Istituto Nazionale di Fisica Nucleare, Sezione di Padova-Trento, [z] University of Padova, I-35131 Padova, Italy
[45] LPNHE, Universite Pierre et Marie Curie/IN2P3-CNRS, UMR7585, Paris, F-75252 France
[46] University of Pennsylvania, Philadelphia, Pennsylvania 19104
[47] Istituto Nazionale di Fisica Nucleare Pisa, [aa] University of Pisa, [bb] University of Siena and [cc] Scuola Normale Superiore, I-56127 Pisa, Italy
[48] University of Pittsburgh, Pittsburgh, Pennsylvania 15260
[49] Purdue University, West Lafayette, Indiana 47907
[50] University of Rochester, Rochester, New York 14627
[51] The Rockefeller University, New York, New York 10021
[52] Istituto Nazionale di Fisica Nucleare, Sezione di Roma 1, [dd] Sapienza Università di Roma, I-00185 Roma, Italy
[53] Rutgers University, Piscataway, New Jersey 08855
[54] Texas A&M University, College Station, Texas 77843
[55] Istituto Nazionale di Fisica Nucleare Trieste/Udine, I-34100 Trieste, [ee] University of Trieste/Udine, I-33100 Udine, Italy
[56] University of Tsukuba, Tsukuba, Ibaraki 305, Japan
[57] Tufts University, Medford, Massachusetts 02155
[58] Waseda University, Tokyo 169, Japan
[59] Wayne State University, Detroit, Michigan 48201
[60] University of Wisconsin, Madison, Wisconsin 53706
[61] Yale University, New Haven, Connecticut 06520

We report a set of measurements of particle production in inelastic $p\bar{p}$ collisions collected with a minimum-bias trigger at the Tevatron Collider with the CDF II experiment. The inclusive charged particle transverse momentum differential cross section is measured, with improved precision, over a range about ten times wider than in previous measurements. The former modeling of the spectrum appears to be incompatible with the high particle momenta observed. The dependence of the charged particle transverse momentum on the event particle multiplicity is analyzed to study the various components of hadron interactions. This is one of the observable variables most poorly reproduced by the available Monte Carlo generators. A first measurement of the event transverse energy sum differential cross section is also reported. A comparison with a PYTHIA prediction at the hadron level is performed. The inclusive charged particle differential production cross section is fairly well reproduced only in the transverse momentum range available from previous measurements. At higher momentum the agreement is poor. The transverse energy sum is poorly reproduced over the whole spectrum. The dependence of the charged particle transverse momentum on the particle multiplicity needs the introduction of more sophisticated particle production mechanisms, such as multiple parton interactions, in order to be better explained.

PACS numbers:

*Deceased

†With visitors from [a] University of Massachusetts Amherst,

## I. INTRODUCTION

In hadron collisions, hard interactions are theoretically well defined and described as collisions of two incoming partons along with softer interactions from the remaining partons. The so-called "minimum-bias" (MB) interactions, on the contrary, can only be defined through a description of the experimental apparatus that triggers the collection of the data. Such a trigger is set up so as to collect, with uniform acceptance, events from all possible inelastic interactions. A description of the MB trigger used in this analysis is given in Sec. III. At the energy of the Tevatron, MB data consist largely of the softer inelastic interactions. In this paper, only the inelastic particle production in the central part of the region orthogonal to the beam axis is exploited. The diffractive interactions are neglected. An exhaustive description of inelastic non-diffractive events can only be accomplished by a non-perturbative phenomenological model such as that made available by the PYTHIA Monte Carlo generator.

The understanding of softer physics is interesting not only in its own right, but is also important for precision measurements of hard interactions in which soft effects need to be accounted for. For example, an interesting discussion on how non-perturbative color reconnection effects between the underlying event and the hard scattering partons may affect the top quark mass measurement can be found in [1]. Also, effects due to multiple parton-parton interactions must be accounted for in MB measurements. A detailed understanding of MB interactions is especially important in very high luminosity environments (such as at the Large Hadron Collider) where a large number of such interactions is expected in the same bunch crossing. MB physics offers a unique ground for studying both the theoretically poorly understood softer phenomena and the interplay between the soft and the hard perturbative interactions.

The observables that are experimentally accessible in the MB final state, namely the particle inclusive distributions and correlations, represent a complicated mixture of different physics effects such that most models could readily be tuned to give an acceptable description of each single observable, but not to describe simultaneously the entire set. The PYTHIA Tune A [2] event generator is, to our knowledge, the first model that comes close to describing a wide range of MB experimental distributions.

In this paper three observables of the final state of antiproton-proton interactions measured with the CDF detector at $\sqrt{s} = 1.96$ TeV are presented: 1) the inclusive charged particle transverse momentum ($p_T$) [3] differential cross section, 2) the transverse energy sum ($\sum E_T$) differential cross section, and 3) the dependence of the charged particle average transverse momentum on the charged particle multiplicity, $C_{\langle p_T \rangle \text{ vs } N_{ch}}$.

The first two measurements address two of the basic features of inelastic inclusive particle production. The measurement of the event transverse energy sum is new to the field, and represents a first attempt at describing the full final state including neutral particles. In this regard, it is complementary to the charged particle measurement in describing the global features of the inelastic $p\bar{p}$ cross section. In this article, previous CDF measurements [4] [5] are widely extended in range and precision. The single particle $p_T$ spectrum now extends to over 100 GeV/$c$, and enables verification of the empirical modeling [6] of minimum-bias production up to the high $p_T$ production region spanning more than twelve orders of magnitude in cross section. The $C_{\langle p_T \rangle \text{ vs } N_{ch}}$ is one of the variables most sensitive to the combination of the physical effects present in MB collisions, and is also the variable most poorly reproduced by the available Monte Carlo generators. Other soft production mechanisms [7], different from a phenomenological extrapolation of QCD to the non-perturbative region, might show up in the high multiplicity region of $C_{\langle p_T \rangle \text{ vs } N_{ch}}$. Should this be the case, we might expect to observe final-state particle correlations similar to those observed in ion-ion collisions [8].

A comparison with the PYTHIA Monte Carlo generator model [9] is carried out for all the distributions and correlations studied.

The rest of this paper is organized as follows: Sec. II describes the detector components most relevant to this analysis. Section III describes the triggers and the datasets used, including a short description of the Monte Carlo generator tuning, the event selection and the backgrounds. In Sec. IV the methods used to correct the data for detector inefficiency and acceptance are discussed. Section V is devoted to the discussion of the systematic uncertainties. In Sec. VI the results are presented and compared to model predictions.

Amherst, Massachusetts 01003, [b]Universiteit Antwerpen, B-2610 Antwerp, Belgium, [c]University of Bristol, Bristol BS8 1TL, United Kingdom, [d]Chinese Academy of Sciences, Beijing 100864, China, [e]Istituto Nazionale di Fisica Nucleare, Sezione di Cagliari, 09042 Monserrato (Cagliari), Italy, [f]University of California Irvine, Irvine, CA 92697, [g]University of California Santa Cruz, Santa Cruz, CA 95064, [h]Cornell University, Ithaca, NY 14853, [i]University of Cyprus, Nicosia CY-1678, Cyprus, [j]University College Dublin, Dublin 4, Ireland, [k]University of Edinburgh, Edinburgh EH9 3JZ, United Kingdom, [l]University of Fukui, Fukui City, Fukui Prefecture, Japan 910-0017 [m]Kinki University, Higashi-Osaka City, Japan 577-8502 [n]Universidad Iberoamericana, Mexico D.F., Mexico, [o]University of Iowa, Iowa City, IA 52242, [p]Queen Mary, University of London, London, E1 4NS, England, [q]University of Manchester, Manchester M13 9PL, England, [r]Nagasaki Institute of Applied Science, Nagasaki, Japan, [s]University of Notre Dame, Notre Dame, IN 46556, [t]University de Oviedo, E-33007 Oviedo, Spain, [u]Texas Tech University, Lubbock, TX 79609, [v]IFIC(CSIC-Universitat de Valencia), 46071 Valencia, Spain, [w]University of Virginia, Charlottesville, VA 22904, [x]Bergische Universität Wuppertal, 42097 Wuppertal, Germany, [ff]On leave from J. Stefan Institute, Ljubljana, Slovenia,

## II. THE CDF DETECTOR

CDF II is a general purpose detector that combines precision charged particle tracking with projective geometry calorimeter towers. A detailed description of the detector can be found elsewhere [10]. Here we briefly describe the detector components that are relevant to this analysis: the tracking system, the central calorimeters, and the forward luminosity counters.

The tracking system is situated immediately outside the beam pipe and is composed of an inner set of silicon microstrip detectors and an outer drift chamber (COT). The silicon detectors are located between radii of $1.5 < r < 29.0$ cm, and provide precision measurements of the track's impact parameter with respect to the primary vertex. The innermost layer (L00) [11] is single sided, and is attached directly on the beam pipe. Five layers of double-sided silicon microstrips (SVXII) [12] cover the pseudorapidity $|\eta| \leq 2$ region: in each layer one side is oriented at a stereo angle with respect to the beam axis to provide three dimensional measurements. The ISL [13] is located outside SVXII. It consists of one layer of silicon microstrips covering the region $|\eta| < 1$ and of two layers at $1 < |\eta| < 2$ where the COT coverage is incomplete or missing. The COT [14] is a cylindrical open-cell drift chamber with 96 sense wire layers grouped into eight alternating superlayers of stereo and axial wires. Its active volume covers $40 < r < 137$ cm and $|z| < 155$ cm, thus providing fiducial coverage up to $|\eta| \lesssim 1$ to tracks originating within $|z| \leq 60$ cm. Outside the COT, a solenoid provides a 1.4 T magnetic field that allows the particle momenta to be computed from the trajectory curvature. The transverse momentum resolution is $\sigma(p_T)/p_T \simeq 0.1\% \cdot p_T/(\mathrm{GeV}/c)$ for the integrated tracking system and $\sigma(p_T)/p_T \simeq 0.2\% \cdot p_T/(\mathrm{GeV}/c)$ for the COT tracking alone.

Located outside the solenoid, two layers of segmented sampling calorimeters (electromagnetic [15] and hadronic [16]) are used to measure the energy of the particles. In the central region, $|\eta| < 1.1$, the calorimeter elements are arranged in a projective tower geometry of granularity $\Delta\eta \times \Delta\phi \approx 0.11 \times 15^\circ$. The electromagnetic components use lead-scintillator sampling. A multi-wire proportional chamber (CES) is embedded at approximately the depth of the shower maximum. The hadron calorimeter uses iron absorbers and scintillators. At normal incidence the total depth corresponds to about 18 radiation lengths in the electromagnetic calorimeter and 4.5 interaction lengths in the hadronic calorimeter.

The energy resolution of the electromagnetic calorimeter is $\sigma(E_T)/E_T = 14\%/\sqrt{(}E_T(\mathrm{GeV})) \oplus 2\%$ for electromagnetic particles. It is $\sigma(E_T)/E_T = 75\%/\sqrt{(}E_T(\mathrm{GeV})) \oplus 3\%$ for single pions when using both calorimeters.

Two systems of gas Cherenkov counters (CLC) [17], covering the forward regions $3.7 < |\eta| < 4.7$, are used to measure the number of inelastic $p\bar{p}$ collisions per bunch crossing and to determine the luminosity. For triggering purposes only, this analysis exploits a Time-of-Flight detector (TOF) [18] located between the COT and the solenoid at a mean radius of 140 cm. The TOF consists of 216 scintillator bars with photomultipliers at each end and covers roughly $|\eta| < 1$.

## III. DATA SAMPLE AND EVENT SELECTION

This analysis is based on an integrated luminosity of 506 $\mathrm{pb}^{-1}$ collected with the CDF II detector between October 2002 and August 2004. The data were collected with a minimum-bias trigger that operates as follows. An antiproton-proton bunch crossing, signalled by the Tevatron radio frequency, is defined to contain at least one $p\bar{p}$ interaction if there is a coincidence in time of signals in both forward and backward CLC modules. This required coincidence is the start gate of the first-level CDF trigger (Level 1) and is the so-called minimum-bias trigger. CDF uses a three-level trigger system that selects events to be recorded to tape at $\sim 75$ Hz from the bunch crossing rate of approximately 2.5 MHz. The minimum-bias trigger is rate limited at Level 1 in order to keep the Level 3 output at 1 Hz. A total of about $16 \times 10^6$ bunch crossings were recorded.

Part of the analysis also uses data collected with a high multiplicity trigger that selects events that passed the minimum-bias trigger precondition and in addition have a large number of primary charged particles. It functions at Level 1 by selecting events with at least 14 hit bars in the TOF system, a hit being defined as the coincidence of two signals from the photomultipliers at the two ends of each bar. At Level 3 this trigger requires at least 22 reconstructed tracks converging to the event vertex. The threshold of 14 TOF signals was selected as the highest compatible with a fully efficient trigger for events with offline charged particle multiplicity $\geq 22$. The latter threshold was dictated by the statistics available in Run I and the MB expectations in Run II. This data sample consists of about 64000 triggered events.

For transverse energy measurements only, a subsample has been used. Only runs with initial instantaneous luminosity below $50 \times 10^{30}$ $\mathrm{cm}^{-2}\mathrm{s}^{-1}$ have been kept in order to reduce the effects of event pile-up in the calorimeters. The total number of bunch crossings accepted in this subsample is about $11 \times 10^6$. The average instantaneous luminosities of the two samples are roughly $17 \times 10^{30}$ $\mathrm{cm}^{-2}\mathrm{s}^{-1}$ for the energy subsample and $20 \times 10^{30}$ $\mathrm{cm}^{-2}\mathrm{s}^{-1}$ for the full sample.

An offline event selection is applied to the recorded sample of minimum-bias triggered events. Events that contain cosmic-ray candidates, identified by the combination of tracking and calorimeter timing, are rejected. Only those events collected when all the detector components were working correctly are included in the final reduced data sample.

### A. Event Selection

Primary vertices are identified by the convergence of reconstructed tracks along the $z$-axis. All tracks with hits in at least two COT layers are accepted. No efficiency correction is applied to the tracks used for this task. Vertices are classified in several quality classes: the higher the number of tracks and their reconstruction quality (Sec. IV A), the higher the class quality assigned to the vertex. For vertices of lowest quality (mainly vertices with one to three tracks) a requirement that they be symmetric is added, *i.e.* there must be at least one track in both the positive and negative rapidity regions for the vertex to be accepted as primary. In other words, the quantity $|(N^+ - N^-)/(N^+ + N^-)|$, where $N^{\pm}$ is the number of tracks in the positive or negative $\eta$ hemisphere, cannot equal one.

Events are accepted that contain one, and only one, primary vertex in the fiducial region $|z_{vtx}| \leq 40$ cm centered around the nominal CDF $z = 0$ position. This fiducial interval is further restricted to $|z_{vtx}| \leq 20$ cm when measurements with the calorimeter are involved.

The event selection described contains an unavoidable contamination due to multiple vertices when the separation between vertices is less than the vertex resolution in the $z$-coordinate, which is about 3 cm. A correction for this effect is discussed in Sec. VI.

### B. Trigger and Vertex Acceptance

Due to small inefficiencies in the response of the CLC detector, the minimum-bias trigger is affected by some inefficiency. This efficiency has been evaluated by monitoring the trigger with several central high transverse energy triggers, such as those containing a high $p_T$ track, a central high $p_T$ electron, or a central high $E_T$ jet. The results show that the trigger efficiency increases with the increase of some global event variables such as central multiplicity and central sum $E_T$.

On the other hand, the total acceptance (including the efficiency) of the trigger has been measured by comparing it with a sample of zero-bias events collected during the same period. The zero-bias data set is collected without any trigger requirements, simply by starting the data acquisition at the Tevatron radio-frequency signal. The results are in agreement with previous studies [19] and indicate that the efficiency depends on a number of variables, most of which in some way are related to the number of tracks present in the detector: number of beam interactions, number of tracks, instantaneous luminosity and the CLC calibration. We parametrized the dependence on these variables so that a correction can be applied on an event-by-event basis.

The total MB trigger acceptance increases linearly with the instantaneous luminosity. As a function of the number of tracks, the acceptance is well represented by a typical turn-on curve starting at about 20% (two tracks) and reaching its plateau with a value between 97 and 99% for about 15 tracks.

As stated above, the present analysis includes data collected with the high multiplicity trigger previously described. The offline selection for these data is the same as that for the minimum-bias. Events from the high multiplicity trigger are accepted if they have reconstructed charged track multiplicity at Level 3 greater than or equal to 22. This value is a compromise between the desire for larger statistics in the multiplicity region where the cross section drops and the available trigger bandwidth. The trigger efficiency for this multiplicity is higher than 97%.

The primary vertex recognition efficiency for the MB data sample is evaluated in two ways: by comparing the number of expected vertices on the basis of the instantaneous luminosity and by using a Monte Carlo simulation with multiple $p\bar{p}$ interactions. This efficiency was studied as a function of various event variables and found to be roughly flat for $|z| \leq$40 cm, but strongly dependent on the number of interactions in the bunch crossing and on the number of tracks available for vertex clustering. Therefore the efficiency has been parametrized as a function of the number of tracks and of the instantaneous luminosity.

Because of their dependence on the number of tracks in the bunch crossing, a variable closely related to the event particle multiplicity, both the trigger and the vertex efficiencies affect not only the total cross section but also the shape of inclusive distributions. The efficiency values are computed on an event-by-event basis, and are common to all the distributions analyzed.

### C. Backgrounds

Diffractive events, with final-state particles mostly confined in the forward regions, may have some activity in the central region that enters as a background in our sample. By assuming the following indicative values $\sigma_{ci}/\sigma_{sd}/\sigma_{dd}$ =44.4/10.3/7.0 mb for the central-inelastic, single-, and double-diffractive cross sections [20], respectively, and knowing the relative CLC acceptances, we estimate their contribution to the MB cross section to be approximately 6%. Roughly the same conclusion was drawn by analyzing a sample of diffractive events generated with the PYTHIA simulation and passed through a MB trigger simulation. Considering that in about half of the diffractive events no primary vertex is reconstructed, we estimate that diffractive production forms up to 3.4% of our MB sample and is concentrated in the region of low charged particle multiplicity and low $\sum E_T$.

For the energy measurements, the presence of calorimeter towers with significant energy deposits not due to particles originating from the $p\bar{p}$ interaction was checked. In a sample of zero-bias events, after requiring no reconstructed tracks and no signal in the CES, about 0.002 towers per event were found above the pedestal threshold. This number increases with the instantaneous lu-

minosity and is attributed to real particles crossing the calorimeter, probably scattered back from the forward calorimeters. The resulting average energy per event was subtracted from the measurement of each event $\sum E_T$.

### D. The Monte Carlo Sample

A sample of simulated Monte Carlo (MC) events about twice the size of the data was generated with PYTHIA version 6.216 [21], with parameters optimized for the best reproduction of minimum-bias interactions. PYTHIA Tune A [2] describes the MB interactions starting from a leading order QCD $2 \to 2$ matrix element augmented by initial- and final-state showers and multiple parton interactions [22], folded in with CTEQ5L parton distribution functions [23] and the Lund string fragmentation model [24]. To model the mixture of hard and soft interactions, PYTHIA introduces a $\hat{p}_{T^0}$ cut off parameter [25] that regulates the divergence of the 2-to-2 parton-parton perturbative cross section at low momenta. This parameter is used also to regulate the additional parton-parton scatterings that may occur in the same collision. Thus, fixing the amount of multiple-parton interactions (*i.e.*, setting the $p_T$ cut-off) allows the hard 2-to-2 parton-parton scattering to be extended all the way down to $p_T(hard) = 0$, without hitting a divergence. The amount of hard scattering in simulated MB events is, therefore, related to the activity of the so-called underlying event in the hard scattering processes. The final state, likewise, is subject to several effects such as the treatments of the beam remnants and color (re)connection effects. The PYTHIA Tune A results presented here are the predictions, not fits.

The MC sample used for all the efficiency and acceptance corrections was generated with Tune A and $\hat{p}_{T^0} = 1.5$ GeV/$c$. This tuning was found to give the same output as the default ($\hat{p}_{T^0} = 0$) with only slightly better reproduction of the high $p_T$ particles and a somewhat larger particle multiplicity distribution.

The definition of primary particles was to consider all particles with mean lifetime $\tau > 0.3 \times 10^{-10}$ s produced promptly in the $p\bar{p}$ interaction, and the decay products of those with shorter mean lifetimes. With this definition strange hadrons are included among the primary particles, and those that are not reconstructed are corrected for. On the other hand, their decay products (mainly $\pi^{\pm}$ from $K^0_S$ decays) are excluded, while those from heavier flavor hadrons are included.

A run-dependent simulation with a realistic distribution of multiple interactions was employed. Events were fully simulated through the detector and successively reconstructed with the standard CDF reconstruction chain. The simulation includes the CLC detectors used to trigger the MB sample.

The MC sample agrees with data within 10% for inclusive charged particle $p_T$ up to about 20 GeV/$c$ (see Fig. 6), and $\eta$ distributions. A discussion on how well the MC sample reproduces the rest of the data can be found in Sec. VI.

## IV. TRACKING AND ENERGY CORRECTIONS

This section describes the procedures adopted to correct the data for detector inefficiencies and limited acceptance, and for reconstruction errors. First, charged particle tracks are selected in such a way as to remove the main sources of background such as secondary particles and mis-identified tracks (Sec. IV A). The tracking efficiency is then computed for the selected tracks, and an appropriate correction is applied to the data distributions (Sec. IV B). The measurement of $\sum E_T$ requires a careful evaluation of the calorimeter intrinsic response and acceptance, and of other distorting effects, especially in the lower $E_T$ range. A correction for each of these effects is described in Sec. IV C and is applied to the data.

### A. Track Selection and Acceptance

Reconstructed tracks are accepted if they comply with a minimal set of quality selections including a minimum number of hits, both in axial and stereo layers of the COT. These requirements are made more stringent if no hits in the silicon detectors are used.

All tracks are required to originate in a fiducial region in the plane $(d_0; \Delta z)$, where $d_0$ is the nearest distance, projected in the transverse plane, between the track extrapolation and the beam axis; $\Delta z$ is the distance between the point of closest approach of the track to the $z$-axis and the $z$-coordinate of the event vertex. The actual region selected in the $(d_0; \Delta z)$ plane depends on the track itself. Tracks reconstructed including the information from silicon detectors are selected within $d_0 < 0.1$ cm; those reconstructed with no information from the silicon detectors have worse resolution in $d_0$, and are accepted if $d_0 < 0.5$ cm. A similar selection criterion is used along the beam axis: $\Delta z < 1$ cm for tracks with silicon information and $\Delta z < 2$ cm for the remaining tracks. These track selection criteria are used to select primary tracks, and were determined from MC simulation as the ones that maximize the ratio of primary to secondary particles.

As a further requirement, primary charged particles must have a transverse momentum greater than 0.4 GeV/$c$ and pseudorapidity $|\eta| \leq 1$ in order to optimize the efficiency and acceptance conditions. The track sample used in this analysis is therefore very different from the one used to reconstruct the event vertex.

The number of primary charged particles in the event after the above selection is defined as the event multiplicity $N_{ch}$.

### B. Tracking Efficiency

The detector acceptance and the tracker efficiency have been analyzed with the aim of estimating a correction to each inclusive distribution presented in the paper. For each track, the multiplicative correction is computed using MC as

$$C(p_T,\, N_{ch}) = \frac{N^{GEN}_{primary}(p_T,\, N_{ch}) \text{ in } |\eta| < 1}{N^{REC}_{primary}(p_T,\, N_{ch}) \text{ in } |\eta| < 1}\,, \quad (1)$$

where $N^{REC}_{primary}$ is the number of tracks reconstructed as primary and $N^{GEN}_{primary}$ the number of generated primary charged particles. This correction factor includes the track detection and reconstruction efficiency, the correction for the contamination of secondary particles (particle interaction, pair creation), particle decays and mis-identified tracks (in MC, reconstructed tracks that do not match to a generated charged particle).

The tracking efficiency is strongly dependent on the number of tracks with a trajectory passing close to the event vertex. To avoid biases due to an incorrect multiplicity distribution in the MC generator, the correction factor was evaluated, as a function of $p_T$, in ten different ranges of track multiplicity.

The tracking efficiency is the largest contribution to $C$. It is about 70% at $p_T = 0.4$ GeV/$c$ and increases to about 92% at 5 GeV/$c$, where it reaches a plateau.

The fraction of secondary and mis-identified tracks ranges between 1 and 3% over the whole spectrum. The final correction is roughly flat in $\eta$ and $\phi$, and shows two broad peaks in $z$ that correspond to the edges of the silicon detector barrels.

The total correction, as defined in Eq. 1, includes also the smearing correction for very high $p_T$ tracks, where the small curvature may be a source of high dispersion in the reconstructed $p_T$ value, and introduces a significant deviation with respect to the generated $p_T$.

The measured track $p_T$ distribution is corrected by weighting each track that enters the distribution by the correction (computed at the $p_T$ and $N_{ch}$ values corresponding to that specific track) and by the event-related acceptances (trigger and vertex efficiency and diffractive event subtraction described in Sec. III B and III C).

To illustrate the effect of the convolution of all the corrections on the final distribution, the ratio of the fully corrected to the raw distributions is shown in Fig. 1. The correction decreases from 1.6 at $p_T = 0.4$ GeV/$c$ to 1.05 above 100 GeV/$c$.

The $C_{\langle p_T\rangle \text{ vs } N_{ch}}$ dependence (presented in Sec. VI B) requires a specific two step correction procedure. First, for each data point at fixed $N_{ch}$, the correction to the $\langle p_T\rangle$ is evaluated and $\langle p_T\rangle$ is corrected accordingly. In a second step, a correction is applied for the smearing of the multiplicity of the events. Using MC, a matrix is generated that contains the probability $P$ that an event

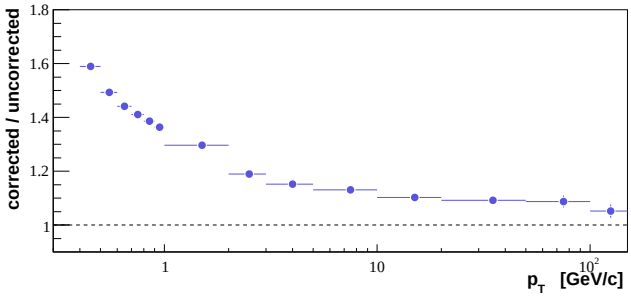


FIG. 1: Ratio of the corrected to uncorrected $p_T$ distributions. The correction is roughly flat for $p_T > 10$ GeV/$c$.

with $n_r$ reconstructed tracks was actually generated with $n_g$ particles:

$$\langle p_T\rangle_{n_r=m} = \sum_{i}^{n_g} (\langle p_T\rangle_{n_r=i} \cdot P^{n_g=i}_{n_r=m})\,, \quad (2)$$

where $m$ and $i$ refer to the reconstructed and generated multiplicity bin, respectively. In doing this it is assumed that, for all multiplicities, the average $p_T$ of events with $n_g = n$ generated tracks is the same as that of the events with $n_r = n$ reconstructed tracks. This is indeed the case after the absolute correction on $\langle p_T\rangle$ is applied.

### C. Calorimeter Response and Correction of the $\sum E_T$ Distribution

The transverse energy is computed in the limited region $|\eta| < 1$ as the scalar sum over the calorimeter towers of the transverse energies in the electromagnetic and hadronic compartments:

$$\sum E_T = \sum_{towers} E_{tower}\ \sin(\theta_{tower})\,, \quad (3)$$

where $\theta_{tower}$ is the polar angle measured with respect to the direction of the proton beam from the actual primary vertex position. Towers with less than 100 MeV deposition are not included in the sum.

CDF calorimetry is optimized for the measurement of high energy depositions and the analysis of its energy response is not usually performed below a few GeV. In this paper the total $\sum E_T$ distribution is pushed down below this limit and a specific study of the energy correction extension had to be done.

The calorimeter response to single charged particles was checked to be well represented by the simulation down to a track $p_T$ of about 400 MeV/$c$. The simulation of the energy deposition of neutral particles is assumed to be correct. Since the fraction of charged and neutral energy produced in data and in our MC sample agree

fairly well, we rely on MC simulation to measure down to $\sum E_T = 1$ GeV the integrated calorimeter response to the total energy deposited.

The list of corrections applied to the data $\sum E_T$ distribution is the following. All corrections are made after the calibration of the calorimeters.

1. Tower relative correction. The response to the energy entering each calorimeter tower was measured with MC as a function of the $\eta$ of the tower and of the $z$ coordinate of the primary vertex and then normalized to the value obtained for the tower with the best response. This correction is introduced to make the calorimeter response flat in $\eta$ and vertex $z$.

2. Absolute correction for the calorimeter response to the total energy released in each event. This is calculated, using MC, as the ratio of the $\sum E_T$ reconstructed in the calorimeter and corrected for the tower relative response in $(\eta; z)$, to the sum of the transverse energies of the generated primary particles in $|\eta| < 1$ whose trajectory extrapolates to the same region. The calorimeter response as a function of $\sum E_T$ is shown in Fig. 2.

3. Correction for the different geometrical acceptance of the calorimeter to events in different positions along the $z$ axis as a function of the $z$ coordinate of the event vertex. This correction ranges from 1 at $z = 0$ to about 0.9 at $|z| = 20$ cm.

4. Correction for undetected charged particles that curl in the magnetic field and do not reach the calorimeter. The average energy due to low $p_T$ charged particles, estimated from MC, as a function of the event $\sum E_T$, is added to each event.

5. Correction for unresolved event pile-up. Our run-dependent MC sample represents well the average number of multiple interactions. This was checked by plotting the ratios of the $\sum E_T$ distributions at high luminosity to the low luminosity ones. A correction was applied by weighting each event by the ratio of the $\sum E_T$ distribution of the events with only one generated interaction to the distribution of events with only one reconstructed interaction. The correction is done for five different ranges of instantaneous luminosity. This weight ranges from about 0.9 to about 1.1.

6. Correction for trigger and vertex acceptance and for contamination of diffractive events described in Sec. III B and III C, respectively. These corrections are applied on an event-by-event basis as weights on the $\sum E_T$ of the events entering the final distribution.

In terms of the calorimeter response (Fig. 2), the region below about 5 GeV is the most critical. The reliability of MC in evaluating the calorimeter response was checked – for charged particles – against the single particle response measured from data. A more detailed discussion can be found in Sec. V D and leads to a systematic uncertainty as high as 15% on the $\sum E_T$ measurement in this region.

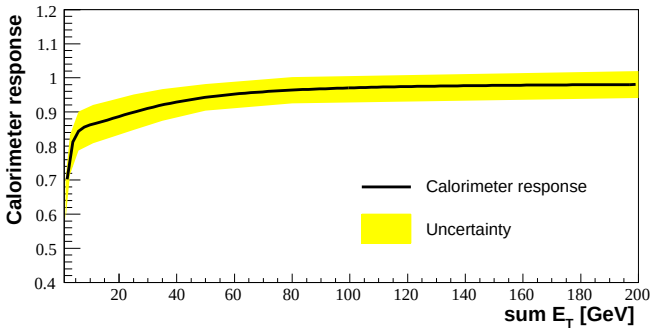


FIG. 2: Calorimeter response as a function of the event $\sum E_T$. The systematic uncertainty is shown as a band.

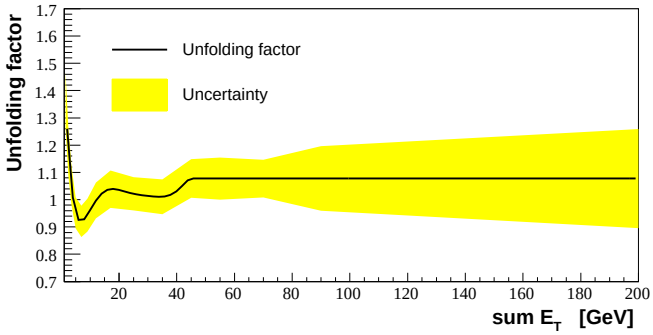


FIG. 3: The unfolding factor of the $\sum E_T$ distribution. The uncertainty is taken as one half of the maximum variation obtained when adding and subtracting the statistical uncertainty to the MC distributions from which the unfolding is computed.

Finally, an unfolding correction for the spread of the events with $\sum E_T$ due to the finite energy resolution is applied. The unfolding is carried out in three steps. (a) An unfolding factor defined as

$$U(E_T^{gen}, E_T^{rec}) = \frac{N_{ev}\left(\sum E_T^{gen}\right)}{N_{ev}\left(\sum E_T^{rec,corrected}\right)}\,, \qquad (4)$$

where *gen* and *rec* indicate respectively the generated and the reconstructed values, is extracted from MC; (b) in order to avoid biases due to the fact that the MC does not perfectly reproduce the data, PYTHIA Tune A is reweighted until it accurately follows the data $\sum E_T$ distribution; (c) a new unfolding factor is computed from the reweighted MC sample and is applied to the corrected data distribution.

The unfolding factor $U$ as a function of the event $\sum E_T$ is shown in Fig. 3. The final corrected $\sum E_T$ distribution is therefore obtained as

$$N_{ev}^{corrected} = \frac{C_5 \cdot U}{C_6} N_{ev}^{raw} \left( \frac{\sum E_T}{C_1 \cdot C_2 \cdot C_3} + C_4 \right) , \quad (5)$$

where $N_{ev}^{corrected}$ and $N_{ev}^{raw}$ refer to the number of events in the corrected and raw distributions respectively. $C_n$ refers to the $n$-th correction in the numeration given above.

## V. SYSTEMATIC UNCERTAINTIES

The selection criteria applied to the dataset, as well as the procedures and the MC generator used to correct for the distortions of the apparatus, efficiency, acceptance limitation, *etc.* are sources of systematic uncertainties. Each source may affect the final distributions in different ways. A description of potential sources of uncertainty, and the methods used to calculate their contributions to the systematic uncertainties on the final results is presented in the following. Table I shows a summary of the systematic uncertainties.

### A. Integrated Luminosity, Trigger Efficiency

There is an overall global 6% systematic uncertainty on the effective time-integrated luminosity measurement [26] that is to be added to all the cross section measurements.

Since the trigger uses the same sub-detectors as the luminosity measurement, the uncertainty on the trigger efficiency is already included in the systematic uncertainty on the integrated luminosity measurement.

### B. Vertex Selection and Efficiency

The final cross sections depend on the correction for vertex reconstruction inefficiency that was evaluated with MC. This correction, applied to the MC sample itself, returns a number of reconstructed vertices that differs by 0.2% from the number of generated ones. The variation on the track $p_T$ distribution from this effect is minor: it has a maximum of 0.6% at $p_T = 1$ GeV/$c$ and is negligible above 5 GeV/$c$. On the event $\langle p_T \rangle$ the variation is about 0.5% in the multiplicity region between 1 and 5. On the $\sum E_T$ distribution it is larger: from 2% at $E_T = 1$ GeV to a negligible value above 6 GeV.

### C. Background of Diffractive Events

There are two possible uncertainties on the correction for the contamination of diffractive events: the value of the diffractive cross section with respect to the inelastic non-diffractive one, and the average number of diffractive particles in the COT region. We let the contribution of diffractive events in MB vary from 5 to 7% and the average multiplicity from 1.0 to 1.4 tracks per event. These values are estimates of the contribution of diffractive processes to the inelastic central production. We take as the uncertainty the maximum variation obtained, which is about 30% of the correction itself. The correction piles up in the low multiplicity region. This uncertainty affects the track cross section by $< 0.5\%$ at $p_T < 1$ GeV/$c$, the event $\langle p_T \rangle$ by less than 1% in the first two multiplicity bins, and the $\sum E_T$ cross section by 8 to 1% in $\sum E_T < 10$ GeV.

### D. Uncertainties Related to the MC Generator

The Monte Carlo modeling of any of the kinematic distributions of particles always introduces an uncertainty on the corrections when the data distributions are not well reproduced. To evaluate this uncertainty, a second sample of events was simulated with the same Monte Carlo generator but different tuning (tune DW [27]). This tuning, when employed for MB production, yields less energy per event than both data and Tune A.

The track reconstruction has a small, but non zero, inefficiency in any kinematic variable. The difference produced by different PYTHIA configurations on the final corrected distributions is taken as a systematic uncertainty. We find that the corrected track $p_T$ distribution varies by 1 to 4% and the $C_{\langle p_T \rangle \text{ vs } N_{ch}}$ dependence varies by less than 1%. To avoid biases due to an incorrect multiplicity distribution in the MC generator, the correction was evaluated in different multiplicity bins. We compare the distributions corrected inclusively (integrating over all particle multiplicities) and differentially with respect to the multiplicity, and we find a relative difference of about 1% over the whole $p_T$ spectrum.

Another uncertainty is due to the contamination of secondary particles. To address this effect, our selection (track $d_0$ and $\Delta z$) is varied both in data and MC and the resulting average number of tracks is compared. No significant variations were observed, after correction, on the average multiplicity.

For the energy measurement, the largest uncertainty is due to the simulation of neutral particles, including the detector simulation and the particle generator. There is no way to disentangle these effects, but their combination may be reflected by a different fraction of neutral energy in MC and in data. This, in turn, may affect the global correction since the energy from neutral particles has a higher calorimeter response than the energy from charged particles. The observed difference in neutral fraction from 0.42 to 0.48 (average values) in data, with respect to MC, corresponds to a variation in the calorimeter response to $\sum E_T$ by 2%.

We take the difference between the $\sum E_T$ distributions

| Source/Distribution | $N_{tracks}$ $(p_T)$ | event $\langle p_T \rangle$ | $N_{events}$ $(\sum E_T)$ |
|---|---|---|---|
| Luminosity and Trigger | 6% | — | 6% |
| Vertex | 0 – 0.6% | 0 – 0.5% | 0 – 2% |
| Diffractive events | 0 – 0.5% | 0 – 1% | 0 – 8% |
| MC tuning | 1 – 4 % | $< 1\%$ | 5 – 15% |
| Method | 1% | — | — |
| Lost $E_T$ | — | — | 1% |
| Pile-Up | — | — | 0 – 3% |

TABLE I: Summary of the systematic uncertainties.

corrected with different MC tunings as the uncertainty due to the generator. The uncertainty is about 15% at $E_T < 5$ GeV, drops to about 5% at 10 GeV and then remains roughly constant. Note that, at least in part, this uncertainty includes the previous one concerning the simulation of neutral particles.

The uncertainty on the amount of energy per event due to low $p_T$ looping charged particles depends directly on the generator because the region of lower momenta is difficult to compare to data. The two PYTHIA tunings that we employ give a difference of about 1% in $\sum E_T$ over the whole spectrum, which corresponds to about the same uncertainty on the distribution shape.

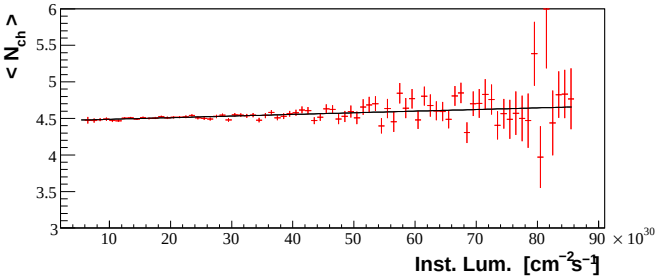


FIG. 4: The raw event average charged particle multiplicity as a function of the instantaneous luminosity. The line represents a linear fit (with slope equal to 0.0022±0.0003). The uncertainty is statistical only.

### E. Uncertainties Originating from Event Pile-Up

Finally, there is an uncertainty due to unresolved pile-up of events within 3 cm to each other along the beam line. None of the algorithms that we tried was able to separate these overlaps efficiently.

The impact on $N_{ch}$ was estimated by comparing the average multiplicity at different instantaneous luminosities and it was found to be $< 0.15$ tracks per event, this being the difference in multiplicity between lowest and highest luminosity regions (Fig. 4). For the uncertainty on the total number of particles in the whole MB sample, we take the difference in multiplicity between the lower and the average luminosity: about 0.04 tracks per event, corresponding to $< 1\%$ of the average raw multiplicity.

The contribution from such events has been taken into account when counting the number of events that enter the cross section calculation (Sec. VI A), but an uncertainty on the correction remains. It amounts to 0.005 tracks per event, which corresponds to a variation of 0.1% of the total MB cross section.

The impact on the average track $p_T$ is negligible; the maximum variation observed when varying the luminosity is about 0.004 GeV/$c$. The uncertainty on the shape of the distribution is therefore negligible.

The effect on $C_{\langle p_T \rangle \text{ vs } N_{ch}}$ is also negligible. This becomes clearer when considering that since the effect on the $p_T$ is almost zero, any variation could only be due to the reallocation of events along the multiplicity axis. The ratio of two plots from samples of high and low luminosities shows negligible variation.

In the case of the energy measurement, the effect of undetected pile-up is much larger and was corrected for (Sec. VI C), but a small uncertainty still remains on the correction itself due to the uncertainty on the calibration of the MC pile-up process.

We may assume that there is no pile-up below a given luminosity (*e.g.*, $10 \times 10^{30}$ cm$^{-2}s^{-1}$) and use this low luminosity sample to compare to our distribution. The ratio of the two is compatible with unity. However, although the pile-up probability in the low luminosity sample is small ($< 1\%$), it is not negligible. We may then assume an uncertainty proportional to that of the MB inelastic non-diffractive cross section used by the MC generator. By assuming conservatively an uncertainty of the MB inelastic non-diffractive cross section used by the MC generator of 6 mb, we calculate that this is equivalent to a variation in the sample average luminosity of $2.5 \times 10^{30}$ cm$^{-2}s^{-1}$, which would be reflected as a $\Delta(\sum E_T)$ of $\pm 0.04$ GeV. This, in turn, corresponds to an uncertainty on the distribution of $< 3\%$ at $E_T = 2$ GeV and negligible at $E_T > 4$ GeV.

### F. Total Systematic Uncertainties

All the sources of uncertainty mentioned in Sec.V add up to the total systematic uncertainty that we attribute to each distribution as shown in the relative plots. Those

| | $p_0$ | $n$ | $s$ | $p_T$ range (GeV/$c$) | $\chi^2/dof$ |
|---|---|---|---|---|---|
| Run 0, 1800 GeV (Eq.8) | 1.29±0.02 | 8.26±0.08 | – | 0.4 - 10. | 102/64 |
| Run 0, 1800 GeV (Eq.8) | 1.29±0.02 | 8.26±0.07 | – | 0.5 - 10. | 90/62 |
| Run 0, 1800 GeV (Eq.8) | 1.3 fixed | 8.28±0.02 | – | 0.4 - 10. | 103/65 |
| Run II, 1960 GeV (Eq.8) | 1.230±0.004 | 8.13±0.01 | – | 0.4 - 10. | 352/192 |
| Run II, 1960 GeV (Eq.8) | 1.223±0.005 | 8.11±0.01 | – | 0.5 - 10. | 258/182 |
| Run II, 1960 GeV (Eq.9) | 1.29±0.02 | 8.30±0.07 | 4.3±0.1 | 0.4 - 150. | 94/233 |
| Run II, 1960 GeV (Eq.9) | 1.36±0.04 | 8.47±0.09 | 4.64±0.07 | 0.5 - 150. | 80/223 |

TABLE II: Comparison of fit parameters with the 1988 data (Run 0). The region $0.4 < p_T < 0.5$ GeV/$c$ in Run 0 data had a large uncertainty on the track efficiency. The two lower rows refer to a fit with the function described in Eq. 9.

originating from MC are added linearly, and their sum is added in quadrature with the others. Uncertainties arising due to the finite MC statistics used to calculate the corrections are represented in the error bars on the data points. For the track $p_T$ distribution, the summed systematic uncertainties range between 3 and 6%, for the $C_{\langle p_T\rangle \text{ vs } N_{ch}}$ correlation from zero to 1.5%, and for the $E_T$ distribution from 5% to 25%. These numbers do not include the 6% uncertainty on the integrated luminosity.

It is worth noting that in this paper the measurements of $p_T$ and $\sum E_T$ spectra are pushed down to very low particle energies. CDF II has limited sensitivity in these regions, so that the correction must necessarily rely heavily on simulation.

## VI. RESULTS

### A. Track $p_T$ Cross Section

The single particle invariant cross section per unit phase-space element is defined as

$$E\frac{d^3\sigma}{dp^3} = \frac{d^3\sigma}{p_T dp_T d\phi dy}\ , \tag{6}$$

where $E$, $p$, and $y$ are the particle energy, momentum, and rapidity, respectively. The charged particle $p_T$ distributions in bins of $\eta$ and $\phi$ have the same shape and mean values. Therefore the cross section factorizes in $\phi$ and $y$ and we may write the invariant $p_T$ differential form as

$$E\frac{d^3\sigma}{dp^3} = \frac{d^3\sigma}{p_T \Delta\phi \Delta y dp_T} = \frac{N_{pcles}/(\varepsilon \cdot A)}{\mathcal{L} p_T \Delta\phi \Delta y dp_T}\ , \tag{7}$$

where $N_{pcles}$ is the raw number of charged particles that is to be corrected for all efficiencies, $\varepsilon$, and acceptance $A$. $\mathcal{L}$ is the effective time-integrated luminosity of the sample.

The accepted region in $\Delta y$ is calculated from the $\eta$ for each charged track, always assuming the charged pion mass. To obtain a number of tracks per unit rapidity interval, each track is weighted by $1/2y$ evaluated at $\eta = 1$. This procedure introduces a bias that could be avoided only by assigning the correct particle mass to all the reconstructed tracks, which is not possible experimentally. Using MC, it was estimated that this bias is at most 5% at $p_T = 0.4$ GeV/$c$, and becomes negligible above 5 GeV/$c$. This estimate has in turn an uncertainty that is difficult to estimate due to the lack of measurements of the relative abundance of particles in MB data.

The acceptance $A$ takes into account the limited $z_{vertex}$ region and the rejection of crossings with detected and undetected pile-up of events. In the latter case the number of undetected events was estimated indirectly by plotting the average $N_{ch}$ as a function of the instantaneous luminosity (Fig. 4). In this plot, the increase in $\langle N_{ch}\rangle$ is due to the increase in number of pile-up events. We assume that virtually no pile-up is present at a luminosity of $\mathcal{L} = 1 \times 10^{30}$ cm$^{-2}$s$^{-1}$. The difference with respect to the $\langle N_{ch}\rangle$ at the average luminosity of the sample yields the estimated number of events that went unobserved. The final acceptance within $|\eta| < 1$ of our event selections for this event sample is $A = 0.595 \pm 0.006$.

The differential cross section is shown in Fig. 5. The same measurement was discussed in [28] and last published by the CDF collaboration in 1988 [4]. For historical reasons, the data published in 1988 were based on the average of positive plus negative tracks, *i.e.* only half of the total tracks were included, which explains most of the scale factor of about 2 between the two measurements. Besides this, the new measurement shows a cross section about 4% higher than the previous one. At least part of this difference may be explained by the increased center-of-mass energy of the collisions from 1800 to 1960 GeV. It should be noted, however, that in 1988 the integrated luminosity was determined indirectly from the UA4 cross section [29] and from the number of events selected. In the region where Run 0 data are available, the distributions have the same shape.

We observe that modeling the particle spectrum with the power-law form used in 1988 to fit the distribution (Eq. 8), does not account for the high $p_T$ tail observed in this measurement (Fig. 5). The form in Eq. 8 is merely empirical, and the $\chi^2$s of the 1988 data fits were already quite poor. Nevertheless, in the limited region up to $p_T = 10$ GeV/$c$, we obtain, for the present data, a set of fit parameters compatible with those published in 1988

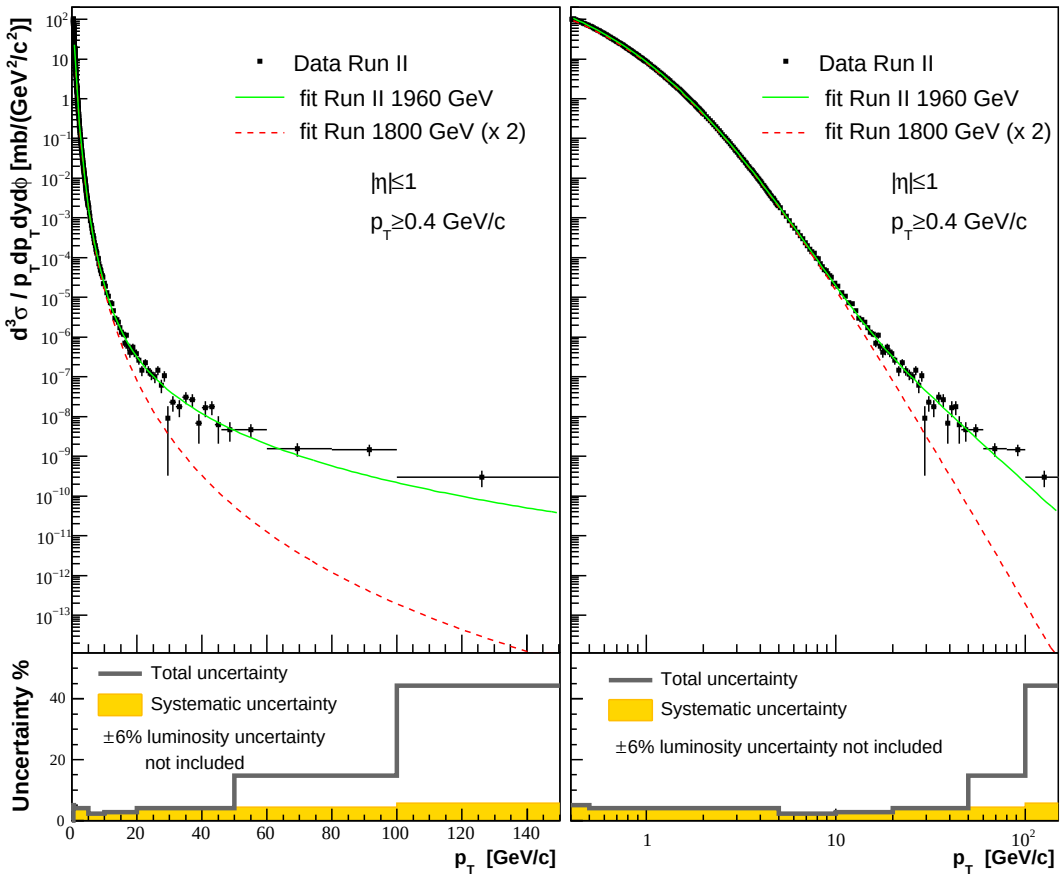


FIG. 5: Left upper plot: the track $p_T$ differential cross section is shown. The error bars describe the uncertainty on the data points. This uncertainty includes the statistical uncertainty on the data and the statistical uncertainty on the total correction. A fit to the functional form in Eq. 8 in the region of $0.4 < p_T < 10$ GeV/$c$ is also shown for the data used in the 1988 analysis [4] at the center of mass energy of 1.8 TeV (dashed line). A fit with a more complicated function (Eq.9) is shown as a continuous line. The plot of data used in the 1988 analysis is scaled by a factor 2 to account for the different normalization. In the plot at the bottom, the systematic and the total uncertainties are shown. The total uncertainty is the quadratic sum of the uncertainty reported on the data points and the systematic uncertainty. The right-hand-side plots show the same distributions but with a logarithmic horizontal scale.

(Table II).

$$f = A\left(\frac{p_0}{p_T + p_0}\right)^n . \tag{8}$$

In our measurement, the tail of the distribution is at least three orders of magnitude higher than what could be expected by simply extrapolating to high $p_T$ the function that fits the low $p_T$ region. In order to fit the whole spectrum, we introduced a more sophisticated parametrization (Eq.9):

$$f = A\left(\frac{p_0}{p_T + p_0}\right)^n + B\left(\frac{1}{p_T}\right)^s . \tag{9}$$

With this new function, we obtain a good $\chi^2$ (see table II) but the data are still not well reproduced above about 100 GeV/$c$.

Figure 6 shows the ratio of data over PYTHIA at hadron level. Also in this case, the data show a larger cross section at high $p_T$ starting from about 20 GeV/$c$. The MC generator does not produce any particles at all beyond 50 GeV/$c$.

### B. Mean $p_T$ vs Event Multiplicity

The dependence of $p_T$ on multiplicity is computed as the average $p_T$ of all charged particles in events with the same charged multiplicity $N_{ch}$, as a function of $N_{ch}$:

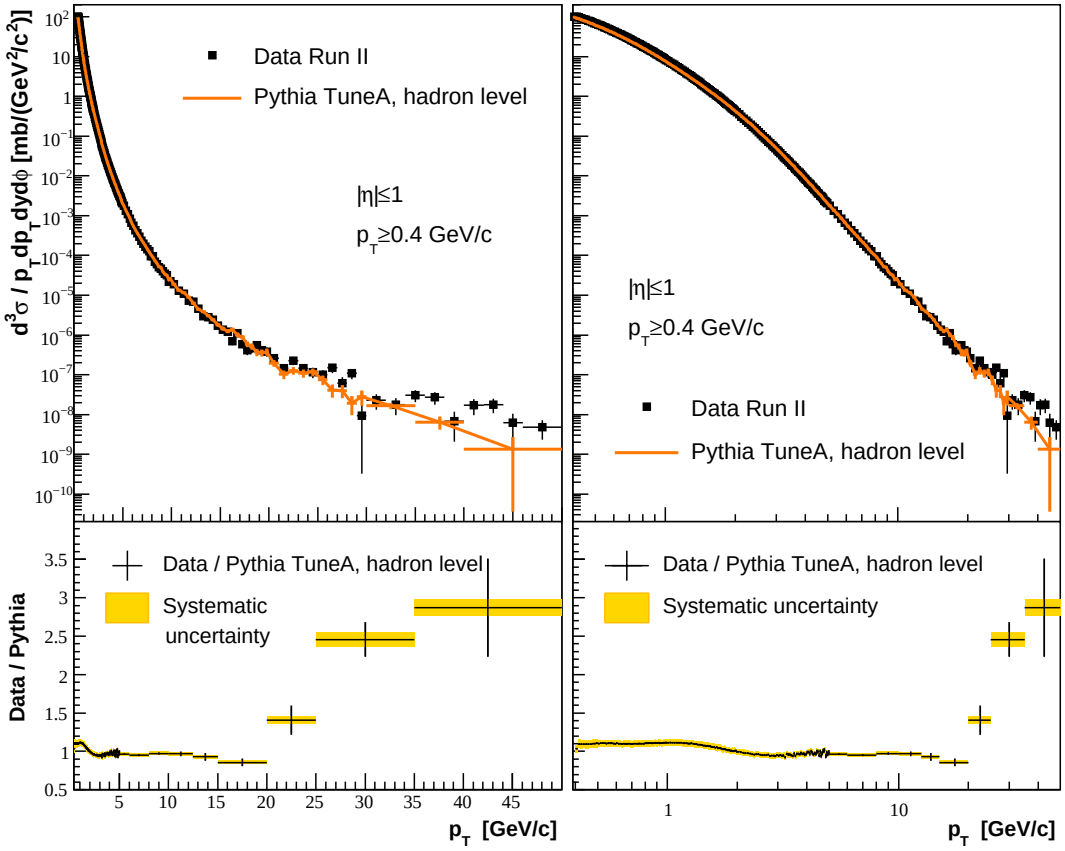


FIG. 6: Left upper plot: comparison of the track $p_T$ differential cross section with PYTHIA prediction at hadron level (Tune A with $\hat{p}_{T0} = 1.5$ GeV/$c$). The data error bars describe the uncertainty on the data points. This uncertainty includes the statistical uncertainty on the data and the statistical uncertainty on the total correction. The ratio of data over prediction is shown in the lower plot. The right-hand-side plots show the same distributions but with a logarithmic horizontal scale. Note that these distributions are cut off at 50 GeV/$c$ since PYTHIA does not produce particles at all beyond that value.

$$C_{\langle p_T\rangle \text{ vs } N_{ch}} = \frac{\sum_{ev}\sum_{i}^{N_{ch}} p_T^i}{N_{ev}^{N_{ch}} \cdot N_{ch}} \,. \qquad (10)$$

The rate of change of $\langle p_T\rangle$ versus $N_{ch}$ is a measure of the amount of hard versus soft processes contributing to minimum-bias collisions; in simulation the rate is sensitive to the modeling of the multiple-parton interactions (MPI) [1]. The model that currently best reproduces the correlation, PYTHIA Tune A, was tuned to fit the activity in the so-called underlying event in high transverse momentum jet production [30]. However, it uses the same cut-off parameter $\hat{p}_{T0}$ to regulate the divergence of the primary 2-to-2 parton-parton scattering and the number of additional parton-parton interactions in the same collision. In addition, in PYTHIA the final state is subject to color (re)connection effects between different parton interactions of the same collision.

The naive expectation from an uncorrelated system of strings decaying to hadrons would be that the $\langle p_T\rangle$ should be independent of $N_{ch}$. However, already at the ISR and at the $Sp\bar{p}S$ [31], and more recently at RHIC and at the Tevatron [28] [32], such flat behavior was convincingly ruled out. A study of the dependence of the mean transverse momentum $\langle p_T\rangle$ on the charged multiplicity was already performed by CDF in Run I and published in [5]. In the analysis presented here an extension to higher multiplicities, well over 40 particles in the central rapidity region, is presented. The precision greatly benefits from the larger statistics obtained with a dedicated trigger (Sec. III). Data from the high multiplicity trigger are included by merging them into the MB sample. Comparison with Run I data (Fig. 7) suggests that there is no faster rise of $\langle p_T\rangle$ at the higher multiplicities. Such a rise could have been considered as an indication of a thermodynamic behavior of an expanding initial state of

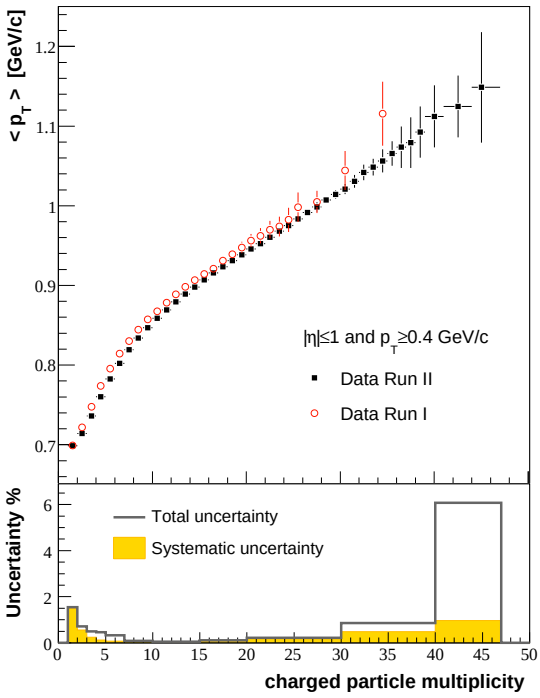


FIG. 7: The dependence of the average track $p_T$ on the event multiplicity. A comparison with the Run I measurement is shown. The error bars in the upper plot describe the uncertainty on the data points. This uncertainty includes the statistical uncertainty on the data and the statistical uncertainty on the total correction. In the lower plot the systematic uncertainty (solid yellow band) and the total uncertainty are shown. The total uncertainty is the quadratic sum of the uncertainty reported on the data points and the systematic uncertainty.

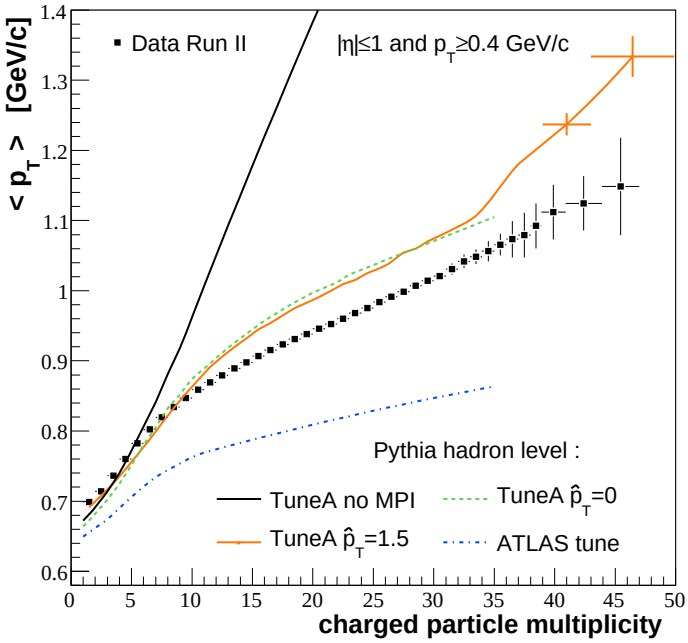


FIG. 8: For tracks with $|\eta| < 1$, the dependence of the average track $p_T$ on the event multiplicity is shown. The error bars on data describe the uncertainty on the data points. This uncertainty includes the statistical uncertainty on the data and the statistical uncertainty on the total correction. A comparison with various PYTHIA tunes at hadron level is shown. Tune A with $\hat{p}_{T0} = 1.5$ GeV/$c$ was used to compute the MC corrections in this analysis (the statistical uncertainty is shown only for the highest multiplicities where it is significant). Tune A with $\hat{p}_{T0} = 0$ GeV/$c$ is very similar to $\hat{p}_{T0} = 1.5$ GeV/$c$. The same tuning with no multiple parton interactions allowed ("no MPI") yields an average $p_T$ much higher than data for multiplicities greater than about 5. The ATLAS tune yields too low an average $p_T$ over the whole multiplicity range.

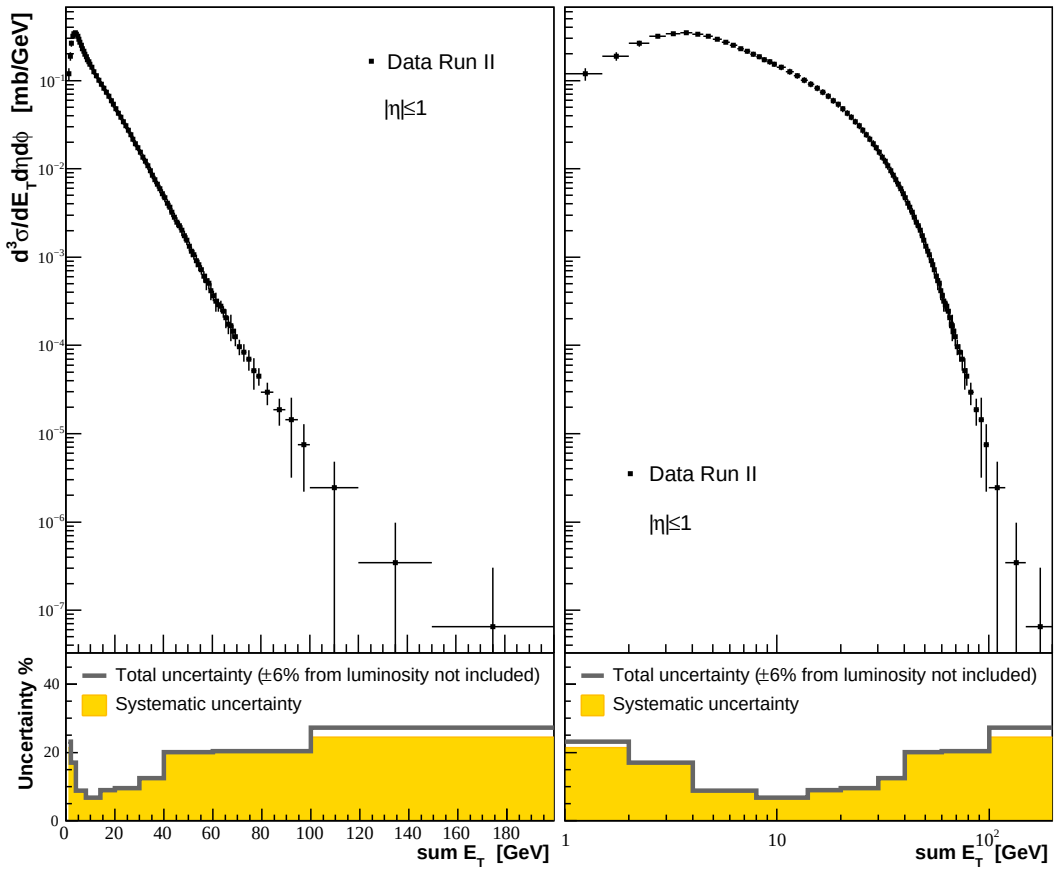


FIG. 9: Left upper plot: the differential $\sum E_T$ cross section in $|\eta| \leq 1$. The error bars describe the uncertainty on the data points. This uncertainty includes the statistical uncertainty on the data and the statistical uncertainty on the total correction. In the bottom plot the systematic (solid band) and the total (continuous line) uncertainties are shown. The total uncertainty is the quadratic sum of the uncertainty reported on the data points and the systematic uncertainty. The right-hand-side plots show the same distributions but with a logarithmic horizontal scale.

hadronic matter [33].

If only two processes contribute to the MB final state, one soft, and one hard (the hard 2-to-2 parton-parton scattering), then demanding large $N_{ch}$ would preferentially select the hard process and lead to a high $\langle p_T \rangle$. However, we see from Fig. 8 (Tune A, no MPI) that with these two processes alone, the average $p_T$ increases much too rapidly. MPI provide another mechanism for producing large multiplicities that are harder than the beam-beam remnants, but not as hard as the primary 2-to-2 hard scattering. By introducing this mechanism, PYTHIA in the Tune A configuration gives a fairly good description of $C_{\langle p_T \rangle \text{ vs } N_{ch}}$ and, although the data are quantitatively not exactly reproduced, there is great progress over fits to Run I data [5]. Note that the systematic uncertainty is always within 2%, a value significantly smaller than the discrepancy with data. PYTHIA Tune A does a better job at describing the data than the ATLAS tune [34]. Both include MPI, but with different choices for the color connections [1]. In Fig. 8, the ATLAS, no MPI and Tune A $\hat{p}_{T^0} = 0$ distributions do not reach multiplicities greater than about 35 solely due to the limited statistics of the generated samples.

### C. $\sum E_T$ Cross Section

The $\sum E_T$ differential cross section is given by

$$\frac{d^3\sigma}{\Delta\phi\Delta\eta dE_T} = \frac{N_{ev}/(\varepsilon \cdot A)}{\mathcal{L}\Delta\phi\Delta\eta dE_T} \,, \tag{11}$$

where $\mathcal{L}$ is the time-integrated luminosity for this subsample of events and $N_{ev}$ is the corresponding corrected number of events. The efficiency $\varepsilon$ includes all trigger and vertex efficiencies and the acceptance $A$ takes into

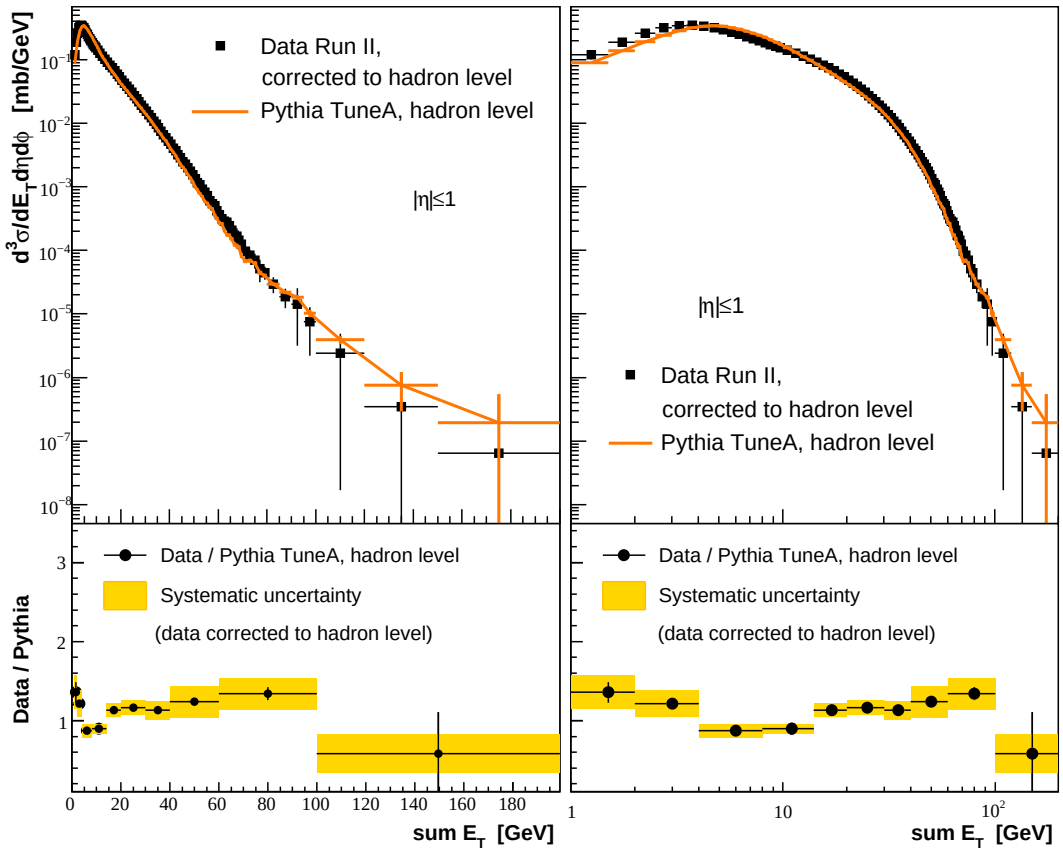


FIG. 10: The left upper plot shows the same data as Fig.9 compared to a PYTHIA prediction at hadron level. The data error bars describe the uncertainty on the data points. This uncertainty includes the statistical uncertainty on the data and the statistical uncertainty on the total correction. The ratio of data to PYTHIA Tune A using $\hat{p}_{T^0} = 1.5$ GeV/$c$ is shown in the lower plot. The right-hand-side plots show the same distributions but with a logarithmic horizontal scale.

account the limited $z$ region ($|z_{vtx}| < 20$ cm for this analysis) and the rejection of crossings with detected and undetected pile-up of events.

The differential cross section in $\sum E_T$ for $|\eta| < 1$ is shown in Fig. 9. The raw and corrected event average transverse energies are $E_T = 7.350 \pm 0.001$(stat.) and $E_T = 10.4 \pm 0.2$(stat.)$\pm 0.7$(syst.) GeV, respectively. This measurement, which represents the total inelastic non-diffractive cross section for events of given $\sum E_T$, is not comparable with previous results since it is the first of its kind at the Tevatron energies.

Figure 10 shows a comparison with the PYTHIA Tune A simulation at hadron level. The simulation does not closely reproduce the data over the whole spectrum. In particular, we observe that the peak of the MC distribution is slightly shifted to higher energies with respect to the data.

## VII. CONCLUSIONS

Minimum-bias collisions are a mixture of hard processes (perturbative QCD) and soft processes (non-perturbative QCD) and, therefore, are very difficult to simulate. They contain soft beam-beam remnants, hard QCD 2-to-2 parton-parton scattering, and multiple parton interactions (soft and hard). To simulate such collisions correctly, the appropriate combination of all the processes involved must be known.

This paper provides a set of high precision measurements of the final state in minimum-bias interactions and compares them to the best available MC model. The following observations may be made:

– The former power-law modeling of the particle $p_T$ spectrum is not compatible with the high momentum tail ($p_T \gtrsim 10$ GeV/$c$) observed in data. The change of slope confirms that the MB spectrum is modeled by the mixing of soft and hard interac-

tions. This distribution may be seen as an indirect measurement of such compositeness. The continuity of the $p_T$ spectrum and of the $C_{\langle p_T \rangle \text{ vs } N_{ch}}$ dependence, and the absence of threshold effects on such a large scale, indicate that there is no clear separation of hard and soft processes other than an arbitrary experimental choice. The more recent tunings of the PYTHIA MC generator (Tune A) reproduce the inclusive charged particle $p_T$ distribution in data within 10% up to $p_T \simeq 20$ GeV/$c$ but the prediction lies below the data at high $p_T$. This may mean that the tune does not have exactly the right fraction of hard 2-to-2 parton-parton scattering and, also, that there is more soft energy in the data than predicted;

– The $\sum E_T$ cross section represents the first attempt to measure the neutral particle activity in MB at CDF. The MC generator tuned to reproduce charged particle production does not closely reproduce the shape of the distribution. This might be related to the observation that there is an excess of energy in the underlying event in high transverse momentum jet production over the prediction of PYTHIA Tune A.

– Among the observables in MB collisions, the dependence of the charged-particle momentum on the event multiplicity seems to be one of the most sensitive variables to the relative contributions by several components of MB interactions. This correlation is reproduced fairly well only with PYTHIA Tune A: the mechanism of multiple parton interactions (with strong final-state correlations among them) has been shown to be very useful in order to reproduce high multiplicity final states with the correct particle transverse momenta. In fact, the data very much disfavor models without MPI, and put strong constraints on multiple-parton interaction models.

The results presented here can be used to improve QCD Monte Carlo models for minimum-bias collisions and further our understanding of multiple parton interactions.

## VIII. ACKNOWLEDGMENTS

We thank the Fermilab staff and the technical staffs of the participating institutions for their vital contributions. This work was supported by the U.S. Department of Energy and National Science Foundation; the Italian Istituto Nazionale di Fisica Nucleare; the Ministry of Education, Culture, Sports, Science and Technology of Japan; the Natural Sciences and Engineering Research Council of Canada; the National Science Council of the Republic of China; the Swiss National Science Foundation; the A.P. Sloan Foundation; the Bundesministerium für Bildung und Forschung, Germany; the Korean Science and Engineering Foundation and the Korean Research Foundation; the Science and Technology Facilities Council and the Royal Society, UK; the Institut National de Physique Nucleaire et Physique des Particules/CNRS; the Russian Foundation for Basic Research; the Ministerio de Ciencia e Innovación, and Programa Consolider-Ingenio 2010, Spain; the Slovak R&D Agency; and the Academy of Finland.

## IX. APPENDIX: DATA TABLES

TABLE III: Data of inclusive charged particle transverse momentum differential cross section (continues across pages).

| $p_T$ (GeV/$c$) | $\sigma$ (mb/(GeV$^2$/$c^2$)) | stat. err. | $p_T$ (GeV/$c$) | $\sigma$ (mb/(GeV$^2$/$c^2$)) | stat. err. |
|---|---|---|---|---|---|
| 0.40 - 0.41 | 1.0145 E+02 | 6.3 E-01 | 2.45 - 2.50 | 1.395 E-01 | 1.5 E-03 |
| 0.41 - 0.42 | 1.0215 E+02 | 6.4 E-01 | 2.50 - 2.55 | 1.243 E-01 | 1.4 E-03 |
| 0.42 - 0.43 | 9.685 E+01 | 6.2 E-01 | 2.55 - 2.60 | 1.111 E-01 | 1.3 E-03 |
| 0.43 - 0.44 | 9.245 E+01 | 6.0 E-01 | 2.60 - 2.65 | 1.004 E-01 | 1.1 E-03 |
| 0.44 - 0.45 | 8.811 E+01 | 5.8 E-01 | 2.65 - 2.70 | 8.97 E-02 | 1.0 E-03 |
| 0.45 - 0.46 | 8.403 E+01 | 5.6 E-01 | 2.70 - 2.75 | 8.232 E-02 | 9.8 E-04 |
| 0.46 - 0.47 | 8.007 E+01 | 5.4 E-01 | 2.75 - 2.80 | 7.325 E-02 | 8.8 E-04 |
| 0.47 - 0.48 | 7.688 E+01 | 5.2 E-01 | 2.80 - 2.85 | 6.656 E-02 | 8.0 E-04 |
| 0.48 - 0.49 | 7.360 E+01 | 5.0 E-01 | 2.85 - 2.90 | 5.952 E-02 | 7.4 E-04 |
| 0.49 - 0.50 | 7.021 E+01 | 4.8 E-01 | 2.90 - 2.95 | 5.390 E-02 | 6.8 E-04 |
| 0.50 - 0.51 | 6.701 E+01 | 4.6 E-01 | 2.95 - 3.00 | 4.949 E-02 | 6.2 E-04 |
| 0.51 - 0.52 | 6.404 E+01 | 4.4 E-01 | 3.00 - 3.05 | 4.475 E-02 | 5.7 E-04 |
| 0.52 - 0.53 | 6.126 E+01 | 4.3 E-01 | 3.05 - 3.10 | 4.070 E-02 | 5.3 E-04 |
| 0.53 - 0.54 | 5.846 E+01 | 4.1 E-01 | 3.10 - 3.15 | 3.698 E-02 | 5.2 E-04 |
| 0.54 - 0.55 | 5.563 E+01 | 3.9 E-01 | 3.15 - 3.20 | 3.345 E-02 | 4.6 E-04 |
| 0.55 - 0.56 | 5.318 E+01 | 3.8 E-01 | 3.20 - 3.25 | 2.994 E-02 | 4.2 E-04 |
| 0.56 - 0.57 | 5.077 E+01 | 3.6 E-01 | 3.25 - 3.30 | 2.824 E-02 | 4.1 E-04 |
| 0.57 - 0.58 | 4.851 E+01 | 3.5 E-01 | 3.30 - 3.35 | 2.549 E-02 | 3.7 E-04 |
| 0.58 - 0.59 | 4.634 E+01 | 3.3 E-01 | 3.35 - 3.40 | 2.349 E-02 | 3.5 E-04 |
| 0.59 - 0.60 | 4.412 E+01 | 3.2 E-01 | 3.40 - 3.45 | 2.123 E-02 | 3.2 E-04 |
| 0.60 - 0.61 | 4.233 E+01 | 3.1 E-01 | 3.45 - 3.50 | 1.932 E-02 | 3.0 E-04 |
| 0.61 - 0.62 | 4.029 E+01 | 3.0 E-01 | 3.50 - 3.55 | 1.808 E-02 | 2.9 E-04 |
| 0.62 - 0.63 | 3.858 E+01 | 2.8 E-01 | 3.55 - 3.60 | 1.634 E-02 | 2.6 E-04 |
| 0.63 - 0.64 | 3.681 E+01 | 2.7 E-01 | 3.60 - 3.65 | 1.532 E-02 | 2.5 E-04 |
| 0.64 - 0.65 | 3.528 E+01 | 2.6 E-01 | 3.65 - 3.70 | 1.402 E-02 | 2.4 E-04 |
| 0.65 - 0.66 | 3.375 E+01 | 2.5 E-01 | 3.70 - 3.75 | 1.282 E-02 | 2.1 E-04 |
| 0.66 - 0.67 | 3.228 E+01 | 2.4 E-01 | 3.75 - 3.80 | 1.193 E-02 | 2.1 E-04 |
| 0.67 - 0.68 | 3.091 E+01 | 2.3 E-01 | 3.80 - 3.85 | 1.092 E-02 | 1.9 E-04 |
| 0.68 - 0.69 | 2.967 E+01 | 2.2 E-01 | 3.85 - 3.90 | 1.009 E-02 | 1.8 E-04 |

| $p_T$ (GeV/$c$) | $\sigma$ (mb/(GeV$^2$/$c^2$)) | stat. err. | $p_T$ (GeV/$c$) | $\sigma$ (mb/(GeV$^2$/$c^2$)) | stat. err. |
|---|---|---|---|---|---|
| 0.69 - 0.70 | 2.829 E+01 | 2.1 E-01 | 3.90 - 3.95 | 9.30 E-03 | 1.7 E-04 |
| 0.70 - 0.71 | 2.715 E+01 | 2.0 E-01 | 3.95 - 4.00 | 8.53 E-03 | 1.6 E-04 |
| 0.71 - 0.72 | 2.601 E+01 | 2.0 E-01 | 4.00 - 4.05 | 8.07 E-03 | 1.5 E-04 |
| 0.72 - 0.73 | 2.499 E+01 | 1.9 E-01 | 4.05 - 4.10 | 7.46 E-03 | 1.5 E-04 |
| 0.73 - 0.74 | 2.392 E+01 | 1.8 E-01 | 4.10 - 4.15 | 6.72 E-03 | 1.4 E-04 |
| 0.74 - 0.75 | 2.293 E+01 | 1.8 E-01 | 4.15 - 4.20 | 6.41 E-03 | 1.3 E-04 |
| 0.75 - 0.76 | 2.204 E+01 | 1.7 E-01 | 4.20 - 4.25 | 5.93 E-03 | 1.2 E-04 |
| 0.76 - 0.77 | 2.115 E+01 | 1.6 E-01 | 4.25 - 4.30 | 5.39 E-03 | 1.1 E-04 |
| 0.77 - 0.78 | 2.027 E+01 | 1.6 E-01 | 4.30 - 4.35 | 5.04 E-03 | 1.1 E-04 |
| 0.78 - 0.79 | 1.943 E+01 | 1.5 E-01 | 4.35 - 4.40 | 4.61 E-03 | 1.0 E-04 |
| 0.79 - 0.80 | 1.871 E+01 | 1.5 E-01 | 4.40 - 4.45 | 4.353 E-03 | 9.8 E-05 |
| 0.80 - 0.81 | 1.803 E+01 | 1.4 E-01 | 4.45 - 4.50 | 4.067 E-03 | 9.6 E-05 |
| 0.81 - 0.82 | 1.727 E+01 | 1.3 E-01 | 4.50 - 4.55 | 3.693 E-03 | 9.2 E-05 |
| 0.82 - 0.83 | 1.655 E+01 | 1.3 E-01 | 4.55 - 4.60 | 3.522 E-03 | 8.4 E-05 |
| 0.83 - 0.84 | 1.594 E+01 | 1.3 E-01 | 4.60 - 4.65 | 3.165 E-03 | 8.1 E-05 |
| 0.84 - 0.85 | 1.533 E+01 | 1.2 E-01 | 4.65 - 4.70 | 3.119 E-03 | 7.8 E-05 |
| 0.85 - 0.86 | 1.469 E+01 | 1.2 E-01 | 4.70 - 4.75 | 2.919 E-03 | 7.4 E-05 |
| 0.86 - 0.87 | 1.415 E+01 | 1.1 E-01 | 4.75 - 4.80 | 2.705 E-03 | 7.1 E-05 |
| 0.87 - 0.88 | 1.361 E+01 | 1.1 E-01 | 4.80 - 4.85 | 2.404 E-03 | 6.5 E-05 |
| 0.88 - 0.89 | 1.313 E+01 | 1.0 E-01 | 4.85 - 4.90 | 2.314 E-03 | 6.3 E-05 |
| 0.89 - 0.90 | 1.258 E+01 | 1.0 E-01 | 4.90 - 4.95 | 2.155 E-03 | 6.0 E-05 |
| 0.90 - 0.91 | 1.212 E+01 | 1.0 E-02 | 4.95 - 5.00 | 2.038 E-03 | 5.8 E-05 |
| 0.91 - 0.92 | 1.1678 E+01 | 9.6 E-02 | 5.00 - 5.20 | 1.784 E-03 | 3.4 E-05 |
| 0.92 - 0.93 | 1.1216 E+01 | 9.4 E-02 | 5.20 - 5.40 | 1.339 E-03 | 2.8 E-05 |
| 0.93 - 0.94 | 1.0829 E+01 | 9.8 E-02 | 5.40 - 5.60 | 1.105 E-03 | 2.3 E-05 |
| 0.94 - 0.95 | 1.0396 E+01 | 9.3 E-02 | 5.60 - 5.80 | 8.392 E-04 | 1.9 E-05 |
| 0.95 - 0.96 | 1.0021 E+01 | 9.1 E-02 | 5.80 - 6.00 | 6.59 E-04 | 1.7 E-05 |
| 0.96 - 0.97 | 9.713 E+00 | 7.9 E-02 | 6.00 - 6.20 | 5.54 E-04 | 1.5 E-05 |
| 0.97 - 0.98 | 9.325 E+00 | 7.6 E-02 | 6.20 - 6.40 | 4.32 E-04 | 1.2 E-05 |
| 0.98 - 0.99 | 9.024 E+00 | 7.4 E-02 | 6.40 - 6.60 | 3.58 E-04 | 1.1 E-05 |
| 0.99 - 1.00 | 8.664 E+00 | 7.0 E-02 | 6.60 - 6.80 | 2.979 E-04 | 9.4 E-06 |
| 1.00 - 1.02 | 8.227 E+00 | 6.4 E-02 | 6.80 - 7.00 | 2.361 E-04 | 8.4 E-06 |
| 1.02 - 1.04 | 7.662 E+00 | 6.0 E-02 | 7.00 - 7.20 | 1.999 E-04 | 7.2 E-06 |
| 1.04 - 1.06 | 7.129 E+00 | 5.6 E-02 | 7.20 - 7.40 | 1.655 E-04 | 6.4 E-06 |
| 1.06 - 1.08 | 6.635 E+00 | 5.3 E-02 | 7.40 - 7.60 | 1.422 E-04 | 5.7 E-06 |
| 1.08 - 1.10 | 6.188 E+00 | 4.9 E-02 | 7.60 - 7.80 | 1.276 E-04 | 5.3 E-06 |
| 1.10 - 1.12 | 5.777 E+00 | 4.6 E-02 | 7.80 - 8.00 | 9.60 E-05 | 4.8 E-06 |
| 1.12 - 1.14 | 5.404 E+00 | 4.4 E-02 | 8.00 - 8.20 | 9.44 E-05 | 4.4 E-06 |
| 1.14 - 1.16 | 5.057 E+00 | 4.0 E-02 | 8.20 - 8.40 | 7.05 E-05 | 3.7 E-06 |
| 1.16 - 1.18 | 4.707 E+00 | 3.8 E-02 | 8.40 - 8.60 | 5.97 E-05 | 3.3 E-06 |
| 1.18 - 1.20 | 4.412 E+00 | 3.6 E-02 | 8.60 - 8.80 | 5.02 E-05 | 3.0 E-06 |
| 1.20 - 1.22 | 4.127 E+00 | 3.4 E-02 | 8.80 - 9.00 | 4.69 E-05 | 2.8 E-06 |
| 1.22 - 1.24 | 3.858 E+00 | 3.2 E-02 | 9.00 - 9.20 | 3.98 E-05 | 2.6 E-06 |
| 1.24 - 1.26 | 3.614 E+00 | 3.0 E-02 | 9.20 - 9.40 | 3.47 E-05 | 2.4 E-06 |
| 1.26 - 1.28 | 3.409 E+00 | 2.8 E-02 | 9.40 - 9.60 | 3.23 E-05 | 2.2 E-06 |
| 1.28 - 1.30 | 3.188 E+00 | 2.7 E-02 | 9.60 - 9.80 | 2.18 E-05 | 1.8 E-06 |
| 1.30 - 1.32 | 2.985 E+00 | 2.5 E-02 | 9.80 - 10.00 | 2.25 E-05 | 1.8 E-06 |
| 1.32 - 1.34 | 2.809 E+00 | 2.4 E-02 | 10.00 - 10.50 | 1.89 E-05 | 1.1 E-06 |
| 1.34 - 1.36 | 2.6298 E+00 | 2.2 E-02 | 10.50 - 11.00 | 1.307 E-05 | 8.6 E-07 |
| 1.36 - 1.38 | 2.476 E+00 | 2.1 E-02 | 11.00 - 11.50 | 1.085 E-05 | 7.5 E-07 |
| 1.38 - 1.40 | 2.325 E+00 | 2.0 E-02 | 11.50 - 12.00 | 7.29 E-06 | 5.9 E-07 |
| 1.40 - 1.42 | 2.192 E+00 | 1.9 E-02 | 12.00 - 12.50 | 6.85 E-06 | 5.7 E-07 |
| 1.42 - 1.44 | 2.053 E+00 | 1.8 E-02 | 12.50 - 13.00 | 4.56 E-06 | 4.4 E-07 |
| 1.44 - 1.46 | 1.939 E+00 | 1.7 E-02 | 13.00 - 13.50 | 2.99 E-06 | 3.5 E-07 |
| 1.46 - 1.48 | 1.822 E+00 | 1.6 E-02 | 13.50 - 14.00 | 2.77 E-06 | 3.3 E-07 |
| 1.48 - 1.50 | 1.725 E+00 | 1.5 E-02 | 14.00 - 14.50 | 2.39 E-06 | 3.0 E-07 |
| 1.50 - 1.52 | 1.624 E+00 | 1.5 E-02 | 14.50 - 15.00 | 1.73 E-06 | 2.5 E-07 |
| 1.52 - 1.54 | 1.536 E+00 | 1.4 E-02 | 15.00 - 15.50 | 1.34 E-06 | 2.1 E-07 |
| 1.54 - 1.56 | 1.441 E+00 | 1.3 E-02 | 15.50 - 16.00 | 1.20 E-06 | 2.0 E-07 |
| 1.56 - 1.58 | 1.358 E+00 | 1.2 E-02 | 16.00 - 16.50 | 7.1 E-07 | 1.5 E-07 |
| 1.58 - 1.60 | 1.287 E+00 | 1.2 E-02 | 16.50 - 17.00 | 1.11 E-06 | 1.8 E-07 |
| 1.60 - 1.62 | 1.212 E+00 | 1.1 E-02 | 17.00 - 17.50 | 5.9 E-07 | 1.3 E-07 |
| 1.62 - 1.64 | 1.153 E+00 | 1.1 E-02 | 17.50 - 18.00 | 4.2 E-07 | 1.1 E-07 |
| 1.64 - 1.66 | 1.084 E+00 | 1.0 E-02 | 18.00 - 18.50 | 4.6 E-07 | 1.1 E-07 |
| 1.66 - 1.68 | 1.0273 E+00 | 9.7 E-03 | 18.50 - 19.00 | 5.5 E-07 | 1.2 E-07 |
| 1.68 - 1.70 | 9.741 E-01 | 9.3 E-03 | 19.00 - 19.50 | 4.2 E-07 | 1.0 E-07 |
| 1.70 - 1.72 | 9.176 E-01 | 8.8 E-03 | 19.50 - 20.00 | 3.84 E-07 | 9.8 E-08 |
| 1.72 - 1.74 | 8.649 E-01 | 8.3 E-03 | 20.00 - 21.00 | 2.61 E-07 | 5.8 E-08 |
| 1.74 - 1.76 | 8.238 E-01 | 8.0 E-03 | 21.00 - 22.00 | 1.45 E-07 | 4.1 E-08 |
| 1.76 - 1.78 | 7.822 E-01 | 7.6 E-03 | 22.00 - 23.00 | 2.27 E-07 | 5.1 E-08 |
| 1.78 - 1.80 | 7.389 E-01 | 7.2 E-03 | 23.00 - 24.00 | 1.45 E-07 | 3.9 E-08 |
| 1.80 - 1.82 | 6.992 E-01 | 6.9 E-03 | 24.00 - 25.00 | 1.16 E-07 | 3.5 E-08 |
| 1.82 - 1.84 | 6.612 E-01 | 6.5 E-03 | 25.00 - 26.00 | 1.00 E-07 | 3.1 E-08 |
| 1.84 - 1.86 | 6.290 E-01 | 6.3 E-03 | 26.00 - 27.00 | 1.48 E-07 | 3.8 E-08 |
| 1.86 - 1.88 | 5.963 E-01 | 6.1 E-03 | 27.00 - 28.00 | 6.20 E-08 | 2.4 E-08 |
| 1.88 - 1.90 | 5.642 E-01 | 5.7 E-03 | 28.00 - 29.00 | 1.08 E-07 | 3.1 E-08 |
| 1.90 - 1.92 | 5.382 E-01 | 5.5 E-03 | 29.00 - 30.00 | 9.2 E-09 | 8.9 E-09 |
| 1.92 - 1.94 | 5.081 E-01 | 5.3 E-03 | 30.00 - 32.00 | 2.28 E-08 | 9.6 E-09 |
| 1.94 - 1.96 | 4.864 E-01 | 5.1 E-03 | 32.00 - 34.00 | 1.77 E-08 | 8.1 E-09 |
| 1.96 - 1.98 | 4.631 E-01 | 4.8 E-03 | 34.00 - 36.00 | 3.07 E-08 | 1.0 E-08 |
| 1.98 - 2.00 | 4.358 E-01 | 4.7 E-03 | 36.00 - 38.00 | 2.69 E-08 | 9.5 E-09 |
| 2.00 - 2.05 | 4.021 E-01 | 3.8 E-03 | 38.00 - 40.00 | 6.8 E-09 | 4.8 E-09 |
| 2.05 - 2.10 | 3.533 E-01 | 3.3 E-03 | 40.00 - 42.00 | 1.69 E-08 | 7.2 E-09 |
| 2.10 - 2.15 | 3.125 E-01 | 3.0 E-03 | 42.00 - 44.00 | 1.77 E-08 | 6.9 E-09 |
| 2.15 - 2.20 | 2.775 E-01 | 2.7 E-03 | 44.00 - 46.00 | 6.2 E-09 | 4.1 E-09 |
| 2.20 - 2.25 | 2.467 E-01 | 2.4 E-03 | 46.00 - 50.00 | 4.7 E-09 | 2.4 E-09 |
| 2.25 - 2.30 | 2.194 E-01 | 2.2 E-03 | 50.00 - 60.00 | 4.7 E-09 | 1.7 E-09 |
| 2.30 - 2.35 | 1.955 E-01 | 2.0 E-03 | 60.00 - 80.00 | 1.55 E-09 | 5.7 E-10 |
| 2.35 - 2.40 | 1.738 E-01 | 1.8 E-03 | 80.00 - 100.00 | 1.49 E-09 | 4.9 E-10 |
| 2.40 - 2.45 | 1.564 E-01 | 1.7 E-03 | 100.00 - 150.00 | 3.0 E-10 | 1.3 E-10 |

TABLE IV: Data of $\langle p_T \rangle$ dependence on multiplicity.

| multiplicity | $\langle p_T \rangle$(GeV/$c$) | stat. err. | multiplicity | $\langle p_T \rangle$(GeV/$c$) | stat. err. |
|---|---|---|---|---|---|
| 1 | 0.6989 | 0.0016 | 22 | 0.9603 | 0.0017 |
| 2 | 0.7141 | 0.0016 | 23 | 0.9681 | 0.0019 |
| 3 | 0.7362 | 0.0016 | 24 | 0.9752 | 0.0024 |
| 4 | 0.7601 | 0.0017 | 25 | 0.9836 | 0.0027 |
| 5 | 0.7826 | 0.0018 | 26 | 0.9916 | 0.0030 |
| 6 | 0.8023 | 0.0018 | 27 | 0.9986 | 0.0057 |
| 7 | 0.8193 | 0.0019 | 28 | 1.0073 | 0.0043 |
| 8 | 0.8341 | 0.0019 | 29 | 1.0143 | 0.0052 |
| 9 | 0.8470 | 0.0003 | 30 | 1.0208 | 0.0063 |
| 10 | 0.8587 | 0.0004 | 31 | 1.0307 | 0.0080 |
| 11 | 0.8694 | 0.0004 | 32 | 1.0419 | 0.0098 |
| 12 | 0.8794 | 0.0005 | 33 | 1.049 | 0.011 |
| 13 | 0.8891 | 0.0006 | 34 | 1.056 | 0.015 |
| 14 | 0.8980 | 0.0006 | 35 | 1.066 | 0.015 |
| 15 | 0.9069 | 0.0007 | 36 | 1.073 | 0.026 |
| 16 | 0.9156 | 0.0008 | 37 | 1.079 | 0.032 |
| 17 | 0.9235 | 0.0008 | 38 | 1.092 | 0.032 |
| 18 | 0.9312 | 0.0010 | 39-40 | 1.112 | 0.039 |
| 19 | 0.9384 | 0.0011 | 41-43 | 1.125 | 0.039 |
| 20 | 0.9457 | 0.0013 | 44-47 | 1.149 | 0.069 |
| 21 | 0.9525 | 0.0015 | | | |

TABLE V: Data of $\sum E_T$ differential cross section.

| $\sum E_T$ range (GeV) | $\sigma$ (mb/GeV) | stat. err. | $\sum E_T$ range (GeV) | $\sigma$ (mb/GeV) | stat. err. |
|---|---|---|---|---|---|
| 1.0 - 1.5 | 1.19e-01 | 1.9e-02 | 37 - 38 | 6.66e-03 | 6.7e-04 |
| 1.5 - 2.0 | 1.89e-01 | 2.1e-02 | 38 - 39 | 5.97e-03 | 6.7e-04 |
| 2.0 - 2.5 | 2.63e-01 | 2.0e-02 | 39 - 40 | 5.24e-03 | 6.2e-04 |
| 2.5 - 3.0 | 3.16e-01 | 1.6e-02 | 40 - 41 | 4.72e-03 | 5.4e-04 |
| 3.0 - 3.5 | 3.41e-01 | 1.2e-02 | 41 - 42 | 4.06e-03 | 4.6e-04 |
| 3.5 - 4.0 | 3.46e-01 | 1.0e-02 | 42 - 43 | 3.67e-03 | 4.8e-04 |
| 4.0 - 4.5 | 3.36e-01 | 1.0e-02 | 43 - 44 | 3.20e-03 | 3.8e-04 |
| 4.5 - 5.0 | 3.17e-01 | 1.1e-02 | 44 - 45 | 2.84e-03 | 3.3e-04 |
| 5.0 - 5.5 | 2.94e-01 | 1.2e-02 | 45 - 46 | 2.50e-03 | 3.3e-04 |
| 5.5 - 6.0 | 2.72e-01 | 1.2e-02 | 46 - 47 | 2.27e-03 | 2.6e-04 |
| 6.0 - 6.5 | 2.50e-01 | 1.2e-02 | 47 - 48 | 2.01e-03 | 2.8e-04 |
| 6.5 - 7.0 | 2.31e-01 | 1.2e-02 | 48 - 49 | 1.75e-03 | 2.4e-04 |
| 7.0 - 7.5 | 2.14e-01 | 1.2e-02 | 49 - 50 | 1.56e-03 | 2.0e-04 |
| 7.5 - 8.0 | 1.99e-01 | 1.2e-02 | 50 - 51 | 1.33e-03 | 1.6e-04 |
| 8.0 - 8.5 | 1.85e-01 | 1.2e-02 | 51 - 52 | 1.16e-03 | 1.6e-04 |
| 8.5 - 9.0 | 1.73e-01 | 1.1e-02 | 52 - 53 | 1.07e-03 | 1.4e-04 |
| 9.0 - 9.5 | 1.63e-01 | 1.1e-02 | 53 - 54 | 9.1e-04 | 1.5e-04 |
| 9.5 - 10 | 1.54e-01 | 1.0e-02 | 54 - 55 | 8.2e-04 | 1.2e-04 |
| 10 - 11 | 1.41e-01 | 1.0e-02 | 55 - 56 | 7.21e-04 | 8.8e-05 |
| 11 - 12 | 1.261e-01 | 9.1e-03 | 56 - 57 | 6.05e-04 | 9.1e-05 |
| 12 - 13 | 1.131e-01 | 8.3e-03 | 57 - 58 | 5.38e-04 | 1.1e-04 |
| 13 - 14 | 1.013e-01 | 7.5e-03 | 58 - 59 | 5.04e-04 | 7.1e-05 |
| 14 - 15 | 9.12e-02 | 6.8e-03 | 59 - 60 | 4.17e-04 | 9.1e-05 |
| 15 - 16 | 8.21e-02 | 6.2e-03 | 60 - 61 | 3.67e-04 | 4.9e-05 |
| 16 - 17 | 7.41e-02 | 5.6e-03 | 61 - 62 | 3.17e-04 | 7.7e-05 |
| 17 - 18 | 6.66e-02 | 5.9e-03 | 62 - 63 | 2.90e-04 | 4.8e-05 |
| 18 - 19 | 5.93e-02 | 4.5e-03 | 63 - 64 | 2.78e-04 | 4.2e-05 |
| 19 - 20 | 5.36e-02 | 4.1e-03 | 64 - 65 | 2.43e-04 | 3.6e-05 |
| 20 - 21 | 4.77e-02 | 3.8e-03 | 65 - 66 | 2.06e-04 | 4.9e-05 |
| 21 - 22 | 4.28e-02 | 3.3e-03 | 66 - 67 | 1.73e-04 | 4.0e-05 |
| 22 - 23 | 3.85e-02 | 3.1e-03 | 67 - 68 | 1.66e-04 | 5.5e-05 |
| 23 - 24 | 3.43e-02 | 2.7e-03 | 68 - 69 | 1.45e-04 | 2.6e-05 |
| 24 - 25 | 3.06e-02 | 2.6e-03 | 69 - 70 | 1.26e-04 | 2.8e-05 |
| 25 - 26 | 2.72e-02 | 2.2e-03 | 70 - 72 | 9.7e-05 | 1.9e-05 |
| 26 - 27 | 2.44e-02 | 2.0e-03 | 72 - 74 | 8.4e-05 | 1.9e-05 |
| 27 - 28 | 2.18e-02 | 1.9e-03 | 74 - 76 | 7.0e-05 | 1.8e-05 |
| 28 - 29 | 1.94e-02 | 1.7e-03 | 76 - 78 | 5.2e-05 | 2.0e-05 |
| 29 - 30 | 1.73e-02 | 1.5e-03 | 78 - 80 | 4.5e-05 | 1.0e-05 |
| 30 - 31 | 1.54e-02 | 1.4e-03 | 80 - 85 | 2.9e-05 | 8.4e-06 |
| 31 - 32 | 1.35e-02 | 1.2e-03 | 85 - 90 | 1.9e-05 | 6.3e-06 |
| 32 - 33 | 1.21e-02 | 1.2e-03 | 90 - 95 | 1.4e-05 | 1.1e-05 |
| 33 - 34 | 1.08e-02 | 1.0e-03 | 95 - 100 | 7.5e-06 | 5.3e-06 |
| 34 - 35 | 9.58e-03 | 9.7e-04 | 100 - 120 | 2.4e-06 | 2.4e-06 |
| 35 - 36 | 8.49e-03 | 8.3e-04 | 120 - 150 | 3.5e-07 | 6.3e-07 |
| 36 - 37 | 7.53e-03 | 8.1e-04 | 150 - 200 | 6.5e-08 | 2.4e-07 |


[1] P. Skands and D. Wicke, Eur. Phys. J. C **52**, 133 (2007).

[2] R. Field, AIP Conf. Proc. **828**, 163 (2006); R. Field, Acta Physica Polonica B **36**, 167 (2005); D. Acosta *et al.* (CDF Collaboration), Phys. Rev. D **70**, 072002 (2004).

[3] In the CDF coordinate system, the origin is the center of the detector and the $z$-axis is along the beam axis. In detector coordinates, $\phi$ is defined to be the azimuthal angle around the beam axis and $\theta$ the polar angle. The radial distance to the beam axis is referred to as $r$. The pseudorapidity $\eta$ is defined as $\eta = -\ln[\tan(\theta/2)]$. The transverse energy and momenta are defined by $E_T = E\sin\theta$ and $p_T = p\sin\theta$ where $E$ is the particle's energy and $p$ the magnitude of its momentum.

[4] F. Abe *et al.* (CDF Collaboration), Phys. Rev. Lett. **61**, 1819 (1988).

[5] D. Acosta *et al.* (CDF Collaboration), Phys. Rev. D **65**, 072005 (2002).

[6] T. Sjöstrand and M. van Zijl, Phys. Rev. D **36**, 2019 (1987) and references therein.

[7] S. Barshay, Phys. Lett. B **127**, 129 (1983); L. Van Hove, Phys. Lett. B **118**, 138 (1982); R. Hagedorn, Rev. Nuovo Cimento **6**, 10 (1983); J. D. Bjorken, Phys. Rev. D **27**, 140 (1983); C. Hwa and X. Wang, Phys. Rev. D **39**, 187 (1989); F. W. Bopp, Phys. Rev. D **33**, 1867 (1986).

[8] T. S. Ullrich *et al.* (STAR Collaboration), Heavy Ion Phys **21**, 143 (2004) and references therein.

[9] T. Sjöstrand, S. Mrenna and P. Skands, J. High Energy Phys. 0605 (2006) 026.

[10] D. Acosta *et al.* (CDF Collaboration), Phys. Rev. D **71**, 032001 (2005); D. Acosta *et al.* (CDF Collaboration), Phys. Rev. D **71**, 052003 (2005); A. Abulencia *et al.* (CDF Collaboration), J. Phys. G Nucl. Part. Phys. **34**, 2457 (2007).

[11] C. S. Hill *et al.*, Nucl. Instrum. Methods A **530**, 1 (2004).

[12] A. Sill *et al.*, Nucl. Instrum. Methods A **447**, 1 (2000).

[13] A. Affolder *et al.*, Nucl. Instrum. Methods A **453**, 84 (2004).

[14] A. Affolder *et al.*, Nucl. Instrum. Methods A **526**, 249 (2004).

[15] L. Balka *et al.*, Nucl. Instrum. Methods A **267**, 272 (1988).

[16] S. Bertolucci *et al.*, Nucl. Instrum. Methods A **267**, 301 (1988).

[17] D. Acosta *et al.*, Nucl. Instrum. Methods A **494**, 57 (2002).

[18] D. Acosta *et al.*, Nucl. Instrum. Methods A **518**, 605 (2004).

[19] D. Acosta *et al.*, Nucl. Instrum. Methods A **461**, 540 (2001).

[20] F. Abe *et al.*, (CDF Collaboration), Phys. Rev. D **50**, 5550 (1994); F. Abe *et al.*, (CDF Collaboration), Phys. Rev. D **50**, 5535 (1994);

[21] T. Sjöstrand *et al.*, High-Energy-Physics Event Generation with PYTHIA 6.1, Comput. Phys. Commun. **135** 238, (2001); T. Sjöstrand, Phys. Lett. B **157**, 321 (1985); T. Sjöstrand and M. van Zijl, Phys. Rev. D **36**, 2019 (1987).

[22] T. Sjöstrand and P. Skands, Eur. Phys. J., C **39**, 129 (2005).

[23] H. L. Lai *et al.* (CTEQ Collaboration), Eur. Phys. J. C **12**, 375 (2000).

[24] B. Andersson, Camb. Monogr. Part. Phys. Nucl. Phys. Cosmol. **7**, 1 (1997).

[25] $\hat{p}_{T^0}$ is defined as the transverse momentum of the 2-to-2 scattering in the rest frame of the hard interaction.

[26] S. Klimenko, J. Konigsberg and T. M. Liss, FERMILAB-FN-0741 (2003).

[27] R. Field, Pub. Proc. 33rd Int. Conf. on High Energy Physics, Moscow, Russia (2006); R. Field, Pub. Proc. TeV4LHC Workshop, Fermilab, Batavia IL, USA (2005).

[28] T. Alexopoulos *et al.* (E735 Collaboration), Phys. Lett. B **336**, 599 (1994); T. Alexopoulos *et al.* (E735 Collaboration), Phys. Rev. Lett. **60**, 1622 (1988).

[29] D. Bernard *et al.* (UA4 Collaboration), Phys. Lett. B **186**, 227 (1987).

[30] A. Affolder *et al.* (CDF Collaboration), Phys.Rev. D **65**, 092002 (2002).

[31] G. Arnison *et al.* (UA1 Collaboration), Phys. Lett. B **118**, 167 (1982); A. Breakstone *et al.*, Phys. Lett. B **132**, 463 (1983).

[32] N. Moggi, Nucl. Phys. Proc. Suppl. B **71**, 221 (1999); T. Alexopoulus *et al.*, Phys. Rev. D **48**, 984 (1993); S. H. Oh, Nucl. Phys. Proc. Suppl. B **25**, 40 (1992).

[33] J. D. Bjorken, Phys. Rev. D **27**, 140 (1983).

[34] C. M. Butter *et. al.* Acta Phys. Polon. B **35**, 433 (2004).